Summer 2023

Implementation of a 3D Laser Profiler System Into a Non-Contacting Method for RNT & Stress Measurements

Caio Neto Penna

IMPLEMENTATION OF A 3D LASER PROFILER SYSTEM INTO A NON-CONTACTING METHOD FOR RNT & STRESS MEASUREMENTS

by

Caio Neto Penna

Bachelor of Science
Pontifical Catholic University of Rio de Janeiro, 2021

Submitted in Partial Fulfillment of the Requirements

For the Degree of Master of Science in

Civil Engineering

College of Engineering and Computing

University of South Carolina

2023

Accepted by:

Dimitris C. Rizos, Director of Thesis

Robert L. Mullen, Reader

Yu Qian, Reader

Ann Vail, Dean of the Graduate School

DEDICATION

Dedicated to João Batista Neto, who inspired me to pursue my dreams, and encouraged me.

ACKNOWLEDGEMENTS

This work has been partially funded by the Federal Railroad Administration (FRA) under contract 693JJ619C000007. The opinions expressed in this article are solely those of the authors and do not represent the opinions of the funding agency.

ABSTRACT

Continuous welded rail (CWR) is susceptible to the development of internal forces in the rail due to thermal effects that can lead to track buckling. Railroads typically deal with the internal stresses in the rail through the inspection of the rail neutral temperature (RNT) which is the temperature at which the internal force is zero. The existing methods in the industry to measure RNT are contacting, destructive, disruptive to railroad operations, and ineffective. The proposed concept is a promising non-contacting, non-disruptive and reference-free technique to measure RNT and the stress state in the rail. The method is based on the deformation of the CWR, and has been developed, validated, and verified in the laboratories of the University of South Carolina as well as in the field. This work discusses the feasibility of 3D Laser Profilers in the proposed concept for RNT measurements, as it can make the current testing procedure more efficient. The discussion introduces the 3D laser profiler used in this work, its implementation in the method, the validation in laboratory testing, field implementation, and discussion on the results. This study finds that it is feasible to use 3D laser profilers from RNT measurements. In addition, the implementation has been validated in laboratory testing, while field testing revealed issues to be addressed in the next generation prototype. Lastly, the passage of trains during field testing affects RNT measurements regardless of the data acquisition system.

TABLE OF CONTENTS

LIST OF TABLES

LIST OF FIGURES

LIST OF SYMBOLS

T	Temperature
k	Curvature
sx	Longitudinal stress in the rail
sy	Vertical stress in the rail
ex	Longitudinal Strain in the rail
ey	Vertical Strain in the rail
E	Steel's modulus of elasticity
n	Poisson's ratio

LIST OF ABBREVIATIONS

CPU ..... Central Processing Unit

CSV .....Comma-Separated Values

CWR .....Continuous Welded Rail

DIC.....Digital Image Correlation

EMI ..... Electromagnetic Interference

FE ..... Finite Elements

FFT .....Fast Fourier Transformation

FRA.....Federal Railroad Administration

RNT .....Rail Neutral Temperature

CHAPTER 1

INTRODUCTION & OBJECTIVES

1.1 Background

Railroads have been a crucial part of the global and American supply chain and economic development for over two centuries, moving people and goods across the country and beyond. The sustained growth of railway transportation and its industry relies on the infrastructure's status, maintenance, and ability to embrace innovation.

Continuous welded rail (CWR) became the standard in modern railroad track construction in the United States for the past two and a half decades because it requires less maintenance, improves ride quality, and increases rail and rolling stock fatigue life [1]. However, there are no expansion joints in CWR, so track stability due to internal forces becomes a critical problem, especially in extreme ambient temperature conditions, such as hot summer and cold winter. Compressive forces can induce track buckling, while tensile forces can result in rail pull-apart failures whenever these forces exceed threshold values [2]. According to Federal Railroad Administration (FRA), rail buckling was responsible for nineteen derailments and around $11 million in total damage costs in 2022 in the United States [3].

The efficient management of internal forces in CWR is crucial to improving network safety and capacity [2]. A large part of track buckling prevention involves managing the thermal forces to keep them at safe levels [2]. Rail neutral temperature (RNT), or stress-free temperature, is the temperature in which the net stress in the rail is zero. Knowing the rail neutral temperature in continuous welded rail tracks not only allows us to know the rail's stress state but also helps estimate critical temperatures and appropriate ranges for maintenance operations [4].

1.2 Problem Statement

The main challenge in managing the CWR internal forces is the need for practical measurement techniques to estimate the RNT in a non-destructive and non-disruptive manner [2]. The appropriate RNT for part of a CWR track is established during the design phase according to extreme historical temperatures [4] [5]. However, traffic, climate changes, track displacements, and maintenance operations alter the RNT of CWR tracks. Therefore, it is essential to assess this parameter in the field periodically.The technique proposed in [5] is a reference-free method and measurement system for estimating the RNT and the longitudinal rail stress that is non-destructive, with minimal or no service disruptions. It belongs to the broad deformation measurements family, and it assumes that the deformation of the top of the rail is non-uniform and that there are no trains on the track (unloaded condition). The referred deformations on the rail can be measured with the StereoDIC technology and correlated with the RNT [5]. Although StereoDIC is a proven technology and has been successfully implemented into the RNT measurement method [5, 6, 7], it has shortcomings concerning speckling the

target. Application of a speckle is time-consuming and, often it needs to be reapplied in the field if a train passes during testing, delaying the test time. Therefore, there is a need to optimize the test procedure. From that perspective, laser profiling, a well-known technology in the rail industry, has been implemented into the proposed methodology to make the test procedure more efficient since it does not require speckling.

1.3 Objectives

The objective of this thesis is to develop the implementation process of a 3D laser profiler into the RNT measurement methodology proposed in [5]. It describes all the steps from the conception, design, and assembly of the work frame to the field implementation and final configurations of the equipment. Also, it comments on the advantages the equipment brought to the methodology, identifies areas of improvement and lists recommendations for future work.

1.4 Thesis Organization

The thesis is organized as follows:Chapter 2: Presents the current state of knowledge and discusses the application of laser technology in railroad inspection & maintenance.

Chapter 3: Presents the concept development of the novel RNT & stress measurements method.

Chapter 4: Describes the laser profiler technology discussed in this thesis, its configuration, setup, and verification.

Chapter 5: Presents the data acquisition and processing processes.

Chapter 6: Implements the prototype technology system in laboratory testing.

Chapter 7: Implements the prototype technology system in field testing.

Chapter 8: Discusses the findings in the laboratory and field tests.

Chapter 9: Presents the conclusion and provides recommendations for future field implementation

CHAPTER 2

CURRENT STATE OF KNOWLEDGE

This chapter presents the current state of knowledge in RNT and stress measurements method on CWR tracks and the application of laser technologies in the railway industry.

2.1 RNT & Stress Measurements

RNT is the temperature at which the longitudinal stress in the rail is zero [4]. This parameter allows engineers to know the rail stress state and estimate critical temperatures and appropriate ranges for maintenance operations [2]. As mentioned, keeping the thermal forces within a safe is a significant part of track buckling or rail pull-apart prevention [2].

The neutral temperature for a CWR track is established during the design phase based on historical maximum and minimum ambient temperatures of the location at which the rail is installed. Nevertheless, traffic, climate changes, track displacements, and maintenance operations alter the RNT of CWR tracks. Therefore, it is essential to assess this parameter in the field periodically.

Rizos [5], Knopf [6], and Chao [8] presented a comprehensive review on existing technologies to estimate RNT in the field and laboratory environments and outlined benefits and shortcomings. The current section of this chapter presents a

discussion of the literature after their reports [5, 6, 7, 8]. They are grouped by the basic principle as follows: (i) rail cutting, (ii) rail lifting, (iii) deformation measurements, (iv) ultrasonic, (v) x-ray, (vi) piezoelectric/magnetic, (vii) vibration, (viii) electrical impedance, (ix) mechanical, (x) chemical, (xi) highly nonlinear solitary waves [7] [8] . Table 2.1 summarizes the technologies listed by Knopf et al. [7] supplemented by methods found in Enshaeian and Rizzo [9] and recent publications found in the literature.

The disadvantages are associated with the system's complexity, difficulty in implementing it, practicality, cost, and instrumentation demands [7]. Also, some of the methods are destructive and disrupt operations at some level because they demand contact of the equipment with the rail to acquire data [7]. On top of that, other methods require stress-free reference measurements, which are typically not available in the field during inspection services [7].

Table 2.1: RNT estimation techniques found in the literature.

Method	Outline	Shortcomings	Reference
Rail Cutting	Cut rail to release thermal stresses and allow deformations for direct measurements	Time consuming Destructive Disruptive to train operations	Knopf et al. [7] Enshaeian and Rizzo [9]
Rail lifting	Apply vertical force to unclipped rail until reaching a pre-determined distance. RNT is estimated between correlation of the vertical stiffness to the axial force.	Time Consuming Semi-destructive Disruptive to train operations. Rail must be in tension	Knopf et al. [7] Enshaeian and Rizzo [9]

Method	Outline	Shortcomings	Reference
Hole-drilling	Hole drilled in the rail web along the rail neutral axis relieves the stress that can be measured by direct deformation measurements	Semi-destructive Disruptive to train operations. Sensitive to hole sources of error Sensitive to surface strain Potential plastic deformations caused by drilling procedure	Knopf et al. [7] Enshaeian and Rizzo [9]
Deformation measurements	Uses strain gauges or extensometers data to compute stresses based on the deformations	Contacting Instrumentation required. Relies on changing dimensions. Needs stress-free reference measurement.	Knopf et al. [7] Enshaeian and Rizzo [9]
Ultrasonic waves	Changes in ultrasonic wave characteristics propagating in the rail are correlated to the internal stress state	Contacting Needs stress-free reference measurement. Sensitive to material structure/defects Sensitive to rail surface quality Potentially high instrumentation demands.	Knopf et al. [7] Enshaeian and Rizzo [9]
X-ray	The axial stresses are estimated based on the atomic distance of two atomic planes	Measures a small surface volume. Needs stress-free reference measurements. Requires clean rail surface. High instrumentation demands.	Knopf et al. [7] Enshaeian and Rizzo [9]

Method	Outline	Shortcomings	Reference
Magnetic	Barkhausen noise produces a magnetic field. Its permeability is correlated to the longitudinal stress	Time-consuming calibration Reference material measurement Eliminate local surface perturbations. High instrumentation demands. Sensitive to microstructure condition	Knopf et al. [7] Enshaeian and Rizzo [9]
Vibro-elastics	Exciting the rail to obtain vibration modes and correlates it to the axial forces.	High instrumentation demands. High instrumentation accuracy Needs stress-free reference measurement	Knopf et al. [7] Enshaeian and Rizzo [9] Belding M, Enshaeian A, Rizzo P [10] Wu et al. [11]
Piezoelectric	The piezoelectric excites the rail to obtain an EMI response signal from the rail that indicates deformation	Advanced FE calculations Contacting Instrumentation installation High instrumentation demands. Experimental stages	Knopf et al. [7] Enshaeian and Rizzo [9]

2.2 Applications of Laser Scanners in the Railroad Industry

Railways are proven to be an efficient way of transporting goods and people and maintaining the infrastructure in a state of good repair is crucial to the safety of operations and uninterrupted service. With the increasing demand for freight and passenger trains, defects on the track are becoming more critical than ever, which makes track inspection and maintenance a primary concern to the industry [12]. In view of the objectives of this thesis, railway inspection approaches can be classified in two broad categories, i.e., contact, and non-contact methods [13]. Within the technologies implemented in the industry, laser sensors are well known for requiring low labor for operation due to their high degree of automation, reliable results, high precision, and valid non-contact properties [14] [13].

Different technologies of laser sensors in broad applications in the railway industry are reported in the literature, such as laser triangulation sensors [12, 14, 13, 15, 16, 17, 18], laser ultrasonic technology [19, 20, 21, 22], LiDAR [23, 24], and structured light vision [25, 26, 27, 28]. Examples of the applications are rail wear localization, track geometry inspection, gauge inspection, rail flatness assessment, and rail profile measurement. This discussion focuses on literature review on rail profile measurement systems since 2013, since it is closely related to the objectives of this thesis of implementing a 3D laser profiler into a contactless rail inspection technology that accurately acquires the shape of the top of rail.

Aiming to explore the feasibility of 3D techniques on rail inspection, Ye, Stewart, and Roberts proposed a laser-based system to detect defects on the rail [12]. They reported that the system is feasible and can identify distinct types of defects based on laboratory and field tests [12]. Yang, Liu, Yi, and Chen presented an online rail wear inspection method based on revised fast global registration algorithm using laser scanners for rail profile data acquisition. Their findings indicate that their method is more accurate, efficient, and robust than similar techniques found in the literature [14]. To detect defects on the rail profile and study rail wear, Ye J, Stewart E, Zhang D, Chen Q, Thangaraj K, and Roberts C proposed a novel integration of multiple laser sensors to overcome the shadowing effect on the laser scanner. They scan the rail from different angles and combine the partial profiles obtained [7]. The authors reported that compared to existing systems, their solution is inexpensive and provides more independent rail profile measurements [13].

Liu, Li, Ma, and Wang suggested an onboard rail profile dynamic measurement system based on 2D laser scanning to distinguish standard rail profiles from those distorted by the inspection vehicle vibrations. Results indicate that their methodology is faster and more robust than the one implemented, called the Hausdorff distance method [15]. Attivissimo, Danese, Giaquinto, and Sforza proposed an onboard real-time measurement system based on laser sensors' rail and wheel profile data. Their objective is to obtain the conicity, a necessary parameter to study the wheel-rail interaction quality [16].

In addition to research projects in the literature, some companies in the rail industry sell rail profile measurement systems employing laser scanners [17, 18]. Two examples are MERMEC and ENSCO. Therefore, Laser profiling is a valid technique for acquiring rail inspection data based on the publications above. Also, they provide efficient, fast, and robust measurements.

CHAPTER 3

RNT & STRESS MEASUREMENTS

This chapter presents the fundamentals of developing the technique to estimate the RNT and stress state in CRW, discussed in detail in [5, 6, 7].

3.1 Concept Development

Two main hypotheses are the basis of the development of the method: (i) Thermal loads will induce non-uniform deformations on the top of the rail head in the transverse (vertical) direction due to the constraints in the transverse direction imposed by the fastening system and the longitudinal constraints due to the continuity of the rail in the longitudinal direction, as illustrated in Figure 3.1 (a) [7]. (ii) Under thermal loads, the web of the rail at a location between two consecutive ties remains stress-free in the transverse (vertical) direction [7]. Hence, the thermal strain component governs the total transverse strain, ε_y, which solely relies on the temperature change [7]. On the other hand, in the longitudinal direction, the rail constraints prevent thermal deformations, inducing significant thermal stresses [7]. Therefore, the total longitudinal strain, ε_x, becomes negligible since the associated mechanical strain negates the thermal strain, as shown in Figure 3.1(b) [7].

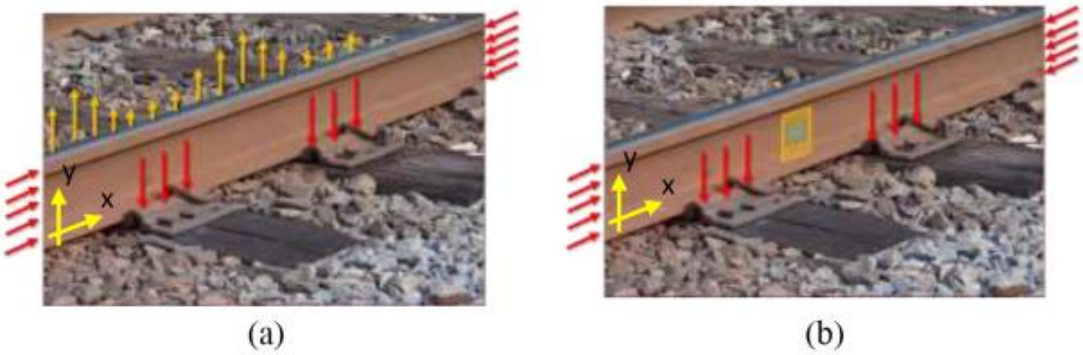

Figure 3.1:Hypotheses schematics: (a) Non-uniform deformation of the top of the rail and (b) Longitudinal and transverse strain of the rail web due to the fastening system constraints (vertical red arrows) and the longitudinal constraints due to the rail continuity (horizontal red arrows). [5, 6, 7]

These hypotheses have been verified and validated by Finite Element Analysis (FEA) and laboratory testing [5, 6, 7]. Also, the authors observed that the curvature of the top of the railhead changes linearly with the temperature and changes sign as the temperature shifts from above to below RNT. Also, the longitudinal strain, ε_x, is negligible and can be considered zero, whereas the longitudinal stress, σ_x, is significant and varies proportionally to the temperature. In contrast, the transverse strain, ε_y, is significant and proportional to temperature changes, while the corresponding stress, σ_y, is negligible and can be considered zero.

These hypotheses and observations led to the formulation of the RNT, and longitudinal stress calculation provided at least two curvature values, k_1, and k_2, of the top of the rail, the strains $(\varepsilon_x, \varepsilon_y)_1$, $(\varepsilon_x, \varepsilon_y)_2$ at the web measured at two different temperatures, T_1 and T_2, as discussed in [5, 6, 7]. The formulation is summarized as follows:

$$RNT = T_2 - k_2\left[\frac{T_2 - T_1}{k_2 - k_1}\right] \tag{3.1}$$

$$T = RNT + \left(\frac{\Delta T}{\Delta \varepsilon y}\right)\varepsilon y \tag{3.2}$$

$$\sigma x \approx \frac{E}{(1+\upsilon)}(\varepsilon x - \varepsilon y) \tag{3.3}$$

The method implementation consists of the following steps: (i) Data acquisition from natural or induced thermal cycles, (ii) RNT estimate and temperature-strain relationship, and (iii) Rail stress state computation. The shape and strain measurements result from the first step, and the implementation of the laser profiler into the method discussed in this work focuses on the top of rail shape measurements to obtain the curvature.

3.2 Measurements Required for the Method Implementation

The shape measurements are the coordinates of the top of rail acquired by a system. To produce reliable results, the acquired height coordinates should be in the order of 10 microns so that the order of the curvature of top of rail is in the order of 10^{-6}(1/mm). In the case the rail temperature is close to the neutral temperature, the curvature of the top of rail might be in the order of 10^{-7}(1/mm). The width of the shape is around 3 inches (the width of the top of rail), and the length depends on the tie spacing of the track. Usually, a acquired length of 12 inches is enough for the purposes of the method.

CHAPTER 4

SYSTEM CONFIGURATION, SETUP & VERIFICATION

This chapter describes the 3D laser profiler implemented in the RNT and stress measurement method. In addition, it discusses the prototype framework setup, the system's configuration, the guidelines to acquired data with the laser, the system's calibration, and lastly, the verification.

4.1 Laser Profiler System

The system employed in this project is the LJ-X8200 2D/3D laser profiler manufactured by Keyence. It is a high-resolution inline measurement system that uses a 2D laser and camera sensor to capture profile section images of the target. Each profile line comprises 3,200 pixels of size twenty-five microns (25 μ). A single 3D surface profile comprises a sequence of up to 16,000 profile lines captured by the 2D laser/camera sensor every twenty-five microns (25 μ) as the relative linear position between the target and the sensor changes. Thus, the grid spacing of the acquired cloud point is twenty-five microns (25 μ), and the size of a single 3D profile at the maximum resolution of the system is eighty millimeters (80 mm) wide and four hundred millimeters (400 mm) long, or 3.15 inch by 15.75 inch. The profiler system captures the out-of-plane deformations within thirty microns (30 μ) accuracy, which is deemed sufficient for the application [7].

Figure 4.1 illustrates the components of the system. The system comprises the laser head sensor (Figure 4.1(a)), the controller (Figure 4.1(b)), and the encoder (Figure 4.1(c),(d)). Furthermore, the power supply (transformer/battery)) in Figure 4.1(e), the data and power cables (Figure 4.1(f)), and the screen (Figure 4.1(g)) are necessary to operate the laser profiler [29].

(a)

(b)

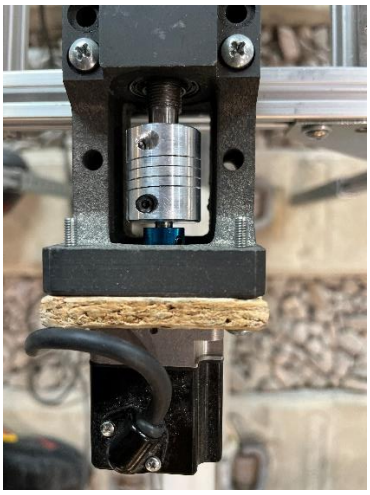

(c)

(d)

(e) (f)

(g)

Figure 4.1: (a) LJ-X Laser head, (b) LJ-X Controller, (c) & (d) Keyence Encoder System, (e) LJ-X Transformer (battery), (f) Keyence LJ-X Cables, (g) Accessories.

The controller is the CPU of the system. It contains the operating system and software for image acquisition and processing in real time, communication ports for data exchange with the laser head, encoder, and external storage devices and ethernet. The 24V/6.5A power supply powers the system. The encoder captures the position and speed of the laser sensor as it scans over the target surface. Lastly, the laser head contains a camera and laser beam to acquire data. The laser head is equipped with blue semiconductor laser, cylindrical lenses, large-aperture receiver lenses, and high-resolution CMOS for high precision and resolution images [30].

Figure 4.2: Laser Profiler System ready to operate in the field.

4.2 Framework Setup

A conventional configuration of the system for 3D profiling applications is based on a stationary laser/camera sensor with the target moving under the laser beam. In the proposed implementation, however, the rail segment to be scanned is fixed to the track and the sensor needs to move linearly over the target surface to enable the 3D capabilities of the system.

Therefore, it is necessary to provide a structure to support the moving laser head as part of the setup to acquire appropriate data with the system. The current hardware setup in the project is an aluminum bar frame with height adjustable legs, illustrated in Figure 4.3. Important parts of the frame are the ball screw, the linear sliders with linear bearings and sliders, the height reference bars, and the steel plate braces at the corners of the frame.

(a)

(b)

(c)

(d)

Figure 4.3: (a) Perspective view, (b) Front view, (c) Lateral View, and (d) Top view of the aluminum Bars frame to support and drive the LJ-X head.

A drill rotates the ball screw to move the laser head over the top of the frame on the sliding bars. The sliding bars provide stability to the laser head to avoid deformations and vibrations of the laser head, avoiding noise in the measurements. A critical part of the frame is the fourteen inches bars at the frame's front and rear, shown in Figure 4.3(b) & (c). They are called height reference bars. The function of the reference bar is to sit on the target, assuring the laser head is in the required position - depicted in Figure 4.2.

According to technical specifications, the top surface of the laser head must sit 34 cm above the target so that it is in the measurement range of the equipment, as shown in Figure 4.4.

It was observed in the laboratory tests that the frame is susceptible to vibration as the screw bar rotates, powered by the drill that drives the laser, introducing noise in the measurements. To solve this problem, the steel plates were attached to the frame's corners.

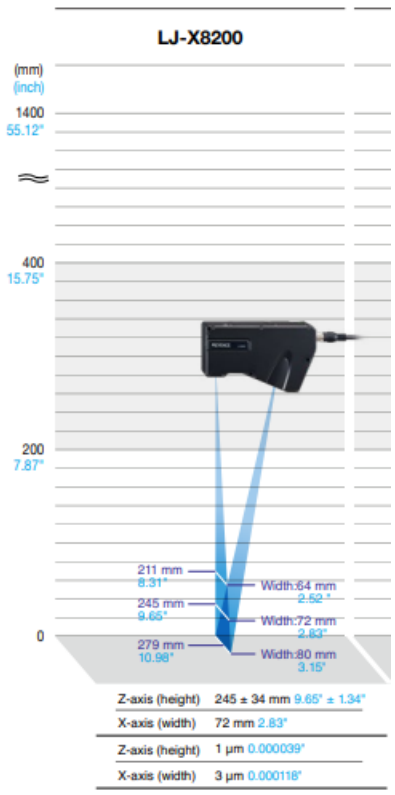

Figure 4.4:Measurement range of the LJ-X8200 3D laser profiler. Reference: Keyence Brochure [31].

4.3 System Configuration

The head and the encoder must be configured to take high quality images and measurements consistent with the needs of the RNT measurement technique. System setup, configuration and calibration was performed by the author with the assistance of the vendor technical support team. A reference image must be acquired with the system to make the necessary adjustments. Reference image is a scan of the target the system will measure in its application. In the case of this project, the reference image is a scan of the top of rail shape. In addition to setting up the head and the encoder, measurement tools and data output must be configured to acquire the desired data for each application. A complete manual with the system configurations used in this project can be found in Annex A. The measurement tools and data output setup will be discussed in this chapter since they are part of the research project.

There are several built-in measurement tools in the controller to return various data to the user [29]. In the discussed application, the continuous profile measurement tool was employed to capture the (X, Y, Z) coordinates of the scanned profiles. Adjustments are still being made to this tool as part of the research project to optimize data acquisition. However, the current configuration of the measurement tool is to return the average peak coordinate - in terms of height - of every three scanned top-of-rail profiles. Thus, since the laser head is set to scan 16000 lines, the controller outputs around 5282 coordinate points.

Hence, the data output is set to export 5300 lines. The remaining eighteen lines are discarded in the processing phase.

Once the final configuration of the head and measurement tools are done, and the encoder is calibrated, the operator must save it in the controller as a program. A program is a set of configurations and measurement tools set by a user. The function of the program is to save the configurations so that the user can operate the system more efficiently. Programs can be changed and saved as needed by the operator. In that case, one does not need to configure it anymore. All it needs is to turn the system on and take the measurements. It is an attractive property of this technology. This includes all the configurations of the system.

4.4 Calibration

The encoder captures the rotation of the ball screw as it spins to drive the laser and sends signals to the controller so it can accurately estimate the position and speed of the laser head and count the scanned lines. Therefore, it needs to be well calibrated, otherwise the images will look compressed or stretched. The encoder calibration is a one-time adjustment.

The encoder of our system was calibrated by the Technical Support specialist assigned to our project using the following procedure. After setting up and turning on the system, in the encoder calibration menu, scan an object with its dimensions known in high precision, and then type the length of the scanned object. The system will associate the scanned distance with the input value, and the encoder is calibrated. For example, to calibrate the encoder with a US five cents coin the operator must scan the coin and type the coin diameter in the encoder calibration menu.

4.5 Guidelines to Operate

Figure 4.5 shows the frame as installed on the track. It is aligned longitudinally with the rail, leveled, and with the reference bar sitting on the top of rail. To acquire reliable data, the frame must sit on a steady base. It is challenging and time consuming to provide steady support for the frame using the ballast stones. Hence, we use two pieces of plywood on the track to stabilize the frame. To finish setting up, the operator must connect the laser sensor and the encoder

to the controller using the cables presented in Figure 4.1, provide power to the system, turn it on, and drive the laser head to the initial position.

Figure 4.5: Frame installed on track ready to acquire measurements.

The starting screen of the system is the “Setup mode”, which is where the user changes the system’s configuration and sets measurement tools. To acquire data, the user must activate the “Run mode”, and start the program with their settings. Once the program is started, the operator must drive the laser head with the drill through the ball screw on the top of the frame from the initial to the final position to scan the profiles. When the laser scans the number of profiles set in the configuration - 16000 in this project case - the controller stops running the program. Lastly, the operator must reset the program in “Run mode” to make the laser ready for the next scan. In the second measurement, it is possible to scan from the final to initial position. Therefore, a single program can acquire multiple scans.

4.6 Flatness Verification

A flatness verification test was run to evaluate the quality of the system configuration. The test consists of scanning a flat granite slab to an accuracy of ten microns and asses the flatness of the granite slab captured by the laser profiler. Figure 4.6 illustrates the test setup.

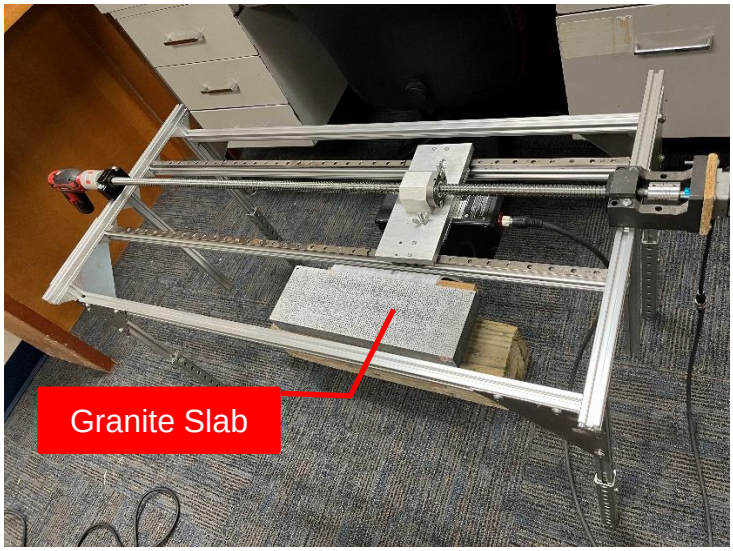

Figure 4.6: Setup of the flatness verification test.

After scanning, the processes consist of exporting profiles in the longitudinal and transverse directions of the granite slab, fit a quadratic curve, and computing the curvature. Since the surface is flat, the curvature is expected to be in the order of 10^{-8} 1/mm.

Figure 4.7 presents the reported profiles. The color maps in the figures represent the height map of the granite slab's flat surface. The granite slab is not perfectly leveled with the floor, explaining the 0.2 mm height difference. Figure 4.8 show the

level measurements of the test setup in the horizontal, vertical, and inclined directions.

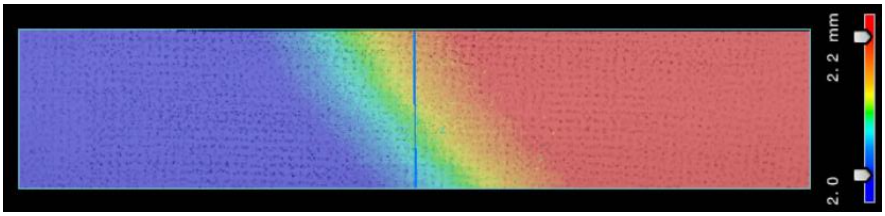

(a)

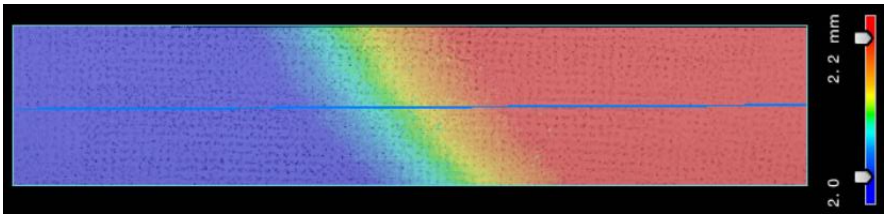

(b)

Figure 4.7: (a) Transverse and (b) Longitudinal profiles evaluated in the granite slab.

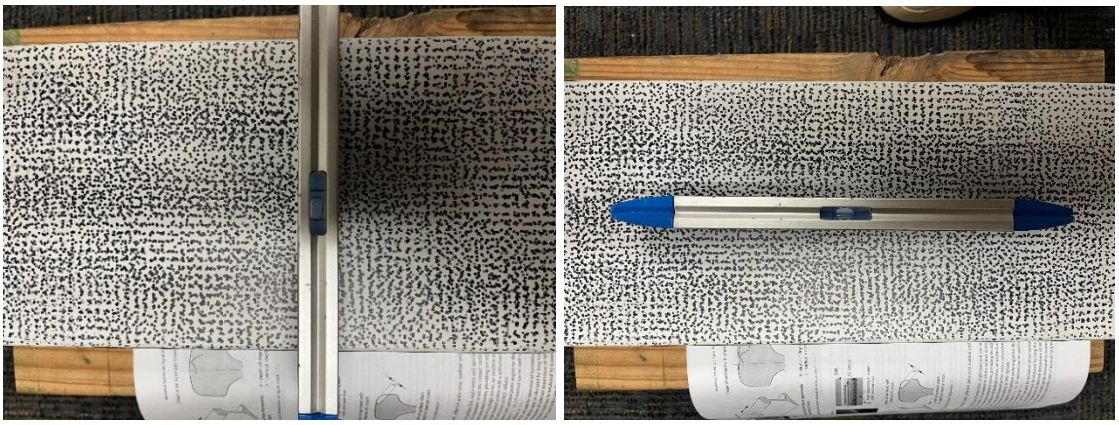

(a) (b)

Figure 4.8: (a) Transverse and (c) Longitudinal level of the granite slab.

Figure 4.9 presents the plot of the acquired profiles and their respective quadratic curve fitting. The reported curvature is of the order of 10^{-8} to 10^{-6} in the longitudinal and transverse directions, respectively. Furthermore, the R^2 of the quadratic fitting in the longitudinal and transverse directions respectively is 0.9992 and 0.9747. The results indicate measurements of a virtually flat surface for all practical purposes. Therefore, the laser profiler could appropriately measure a flat surface, so the configuration presented in this chapter is adequate for acquiring data. The system is now ready for laboratory and field implementation and verification.

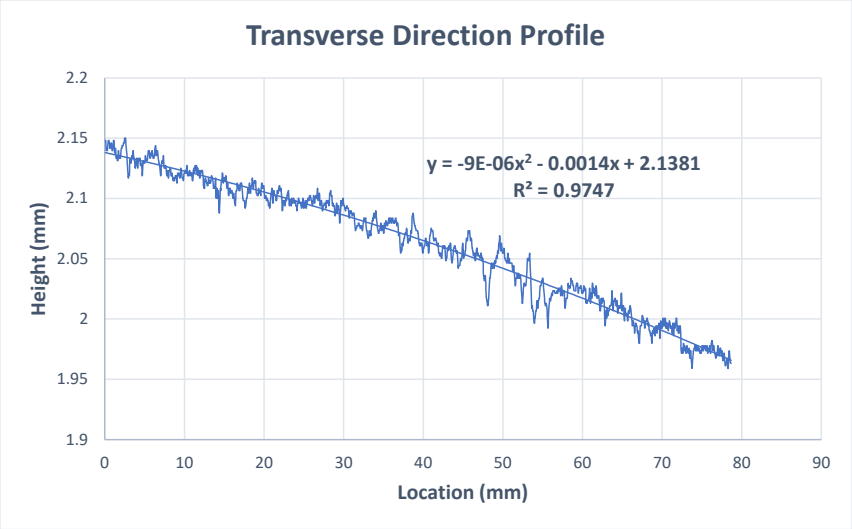

(a)

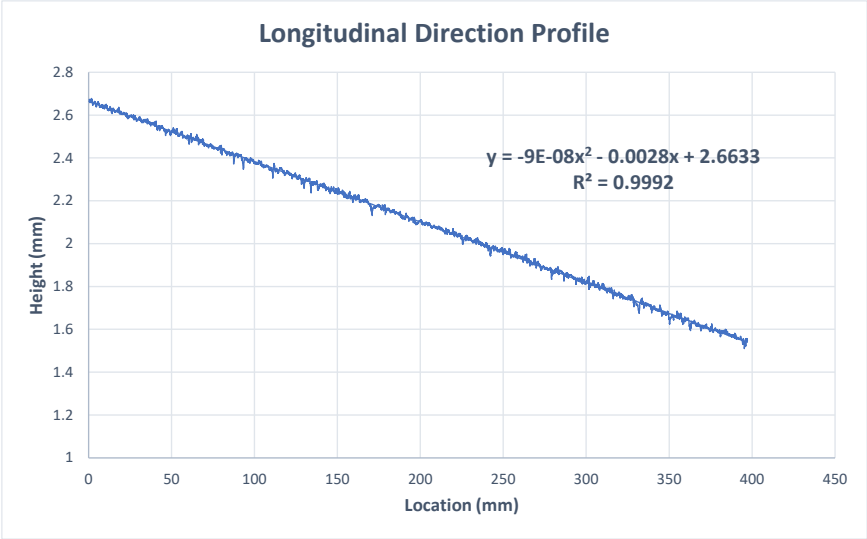

(b)

Figure 4.9: Plot of the (a) Transverse and (b) Longitudinal profiles with their respective quadratic fitting.

CHAPTER 5

DATA ACQUISITION & PROCESSING

This chapter discusses the data acquisition and processing to measure RNT with the 3D laser profiler. Data acquisition consists of taking shape measurements of the top of the rail surface and images of the scanned target. The processing of the data consists of computing the curvature of the top of rail that correlates with temperature at which the data was acquired to measure RNT. If necessary, the processing phase includes applying filters to the data to remove outliers. The purpose of acquiring images of the target is to simulate the data acquisition process in the post processing, if necessary.

5.1 Data Acquisition

The laser profiler is currently set to export the 5300 coordinate points (X, Y, Z) that represent the top of rail's peak, as shown in Figure 5.1. The peak is defined as the line that contains the greatest height values- Z coordinate- in the scanned shape of the top of rail. The objective of exporting the peak is to plot it and compute the curvature that correlates to the temperature. The coordinate points are exported in a CSV file format as shown in Figure 5.2. In Figure 5.2, the second row of the CSV file explains its structure.

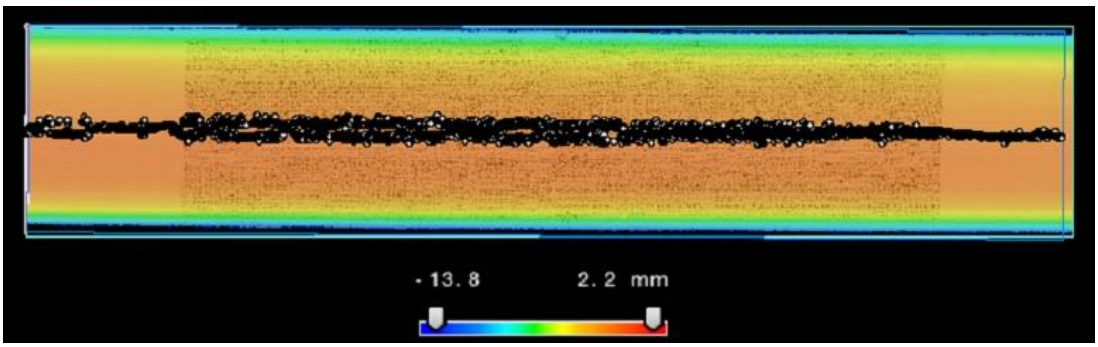

Figure 5.1: Top of Rail peak points in the LJ-X user interface

	A	B	C	D	E	F	G	H	I	J	K	L
1	posxyz	50.53589	2.8349	0.01576	49.43711	2.90471	0.03761	49.31176	2.97911	0.05309	46.93799	3.04289
2	Flag	X1	Y1	Z1	X2	Y2	Z2	X3	Y3	Z3	...	
3												

Figure 5.2: CSV file containing the top of rail peak line

The system exports an image of the top of rail in addition to the CSV file containing the top of rail peak coordinates. The function of the image is simulating the data acquisition process offline and will be discussed in the simulation section of this chapter. Figure 5.3 illustrates the image acquired in one scan.

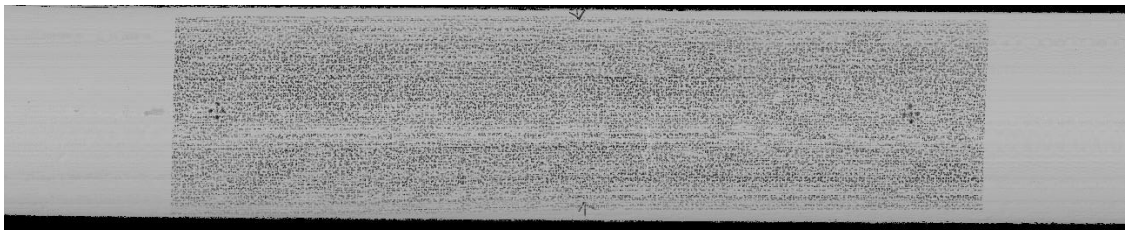

Figure 5.3: Image of the top of rail acquired by the laser profiler system.

An additional way to export the coordinates of the peak line is manually in the “Setup mode” screen, illustrated in figure 5.3. In the “3D observation” tool, it is possible to draw lines in a 2D image of the scanned object and export the height of each profile contained in the drawn line. The reported height line is exported in a CSV file. The “3D observation” tool is shown in Figure 5.4.

The height line in the CSV file is organized with respect to their respective profile index. Therefore, from zero to sixteen thousand. It is necessary to convert from profile index to the location in the longitudinal axis, in millimeters (mm), to accurately compute the curvature. It is known the grid spacing is twenty-five microns (25 μ), so multiply each index by 0.025 millimeters (mm) to convert from profile index to longitudinal axis location. The profile plot with the converted location is presented in Figure 5.5. This manual process can be done during real time acquisition or with offline simulation.

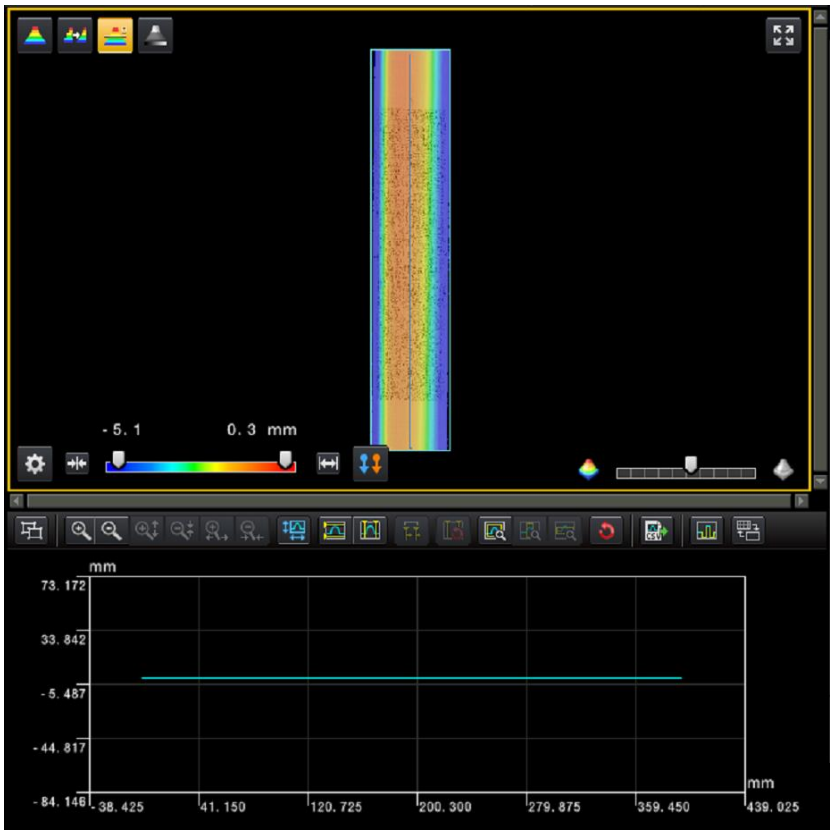

Figure 5.4: 3D Observation tool in the LJ-X8200 “Setup mode” screen.

	C
2	-0.5749
3	-0.5769
4	-0.579
5	-0.5769
6	-0.5728
7	-0.5707
8	-0.5728
9	-0.5769
10	-0.5832
11	-0.5894
12	-0.5915
13	-0.5894
14	-0.5894
15	-0.5873
16	-0.5832
17	-0.579

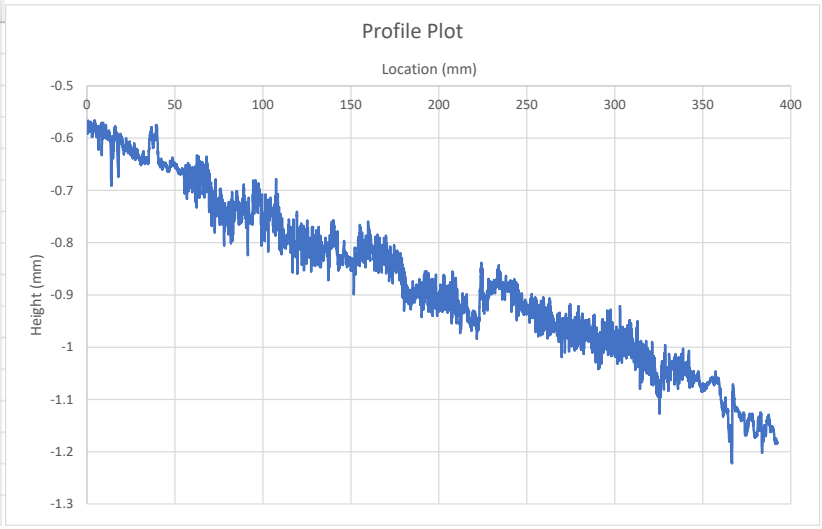

Figure 5.5: Profile Obtained with the 3D observation tool.

5.2 LJ-X Simulation Software

The simulation software is powered by the system manufacturer, and it is the resource that allows offline data acquisition. As in its name, provided the captured image and the programs, the software simulates the laser profiler system allowing the user to process and acquire data offline without the need to install and operate the system in real life. This feature is convenient in our application because once we acquire data in the field, it is difficult and expensive to return to the railroad track and acquire new data with new configurations. However, the simulator makes the alterations possible.

5.3 Data Processing

The first step to obtain the curvature of the top of the rail is rewriting the CSV file in the format illustrated in Figure 5.6. This step is necessary when using excel to process the data and obtain the curvature. Excel reads the csv file and organizes it in a single row, as shown in Figure 5.2. The problem with this structure is that it is not organized in a way that one can easily plot the profile, hence the file is reorganized to obtain the profile conveniently. The python code present in annex B was written to do it.

	A	B	C	D	E	F
1	X	Y	Z		Heading	
2	45.89194	3.18271	0.10556	X1	Y1	Z1
3	46.03919	3.26001	0.11359	X2	Y2	Z2
4	46.03959	3.33502	0.09846	X3	Y3	Z3
5	46.48836	3.41702	0.09375	...	...	...

Figure 5.6: Rewritten CSV file and its structure

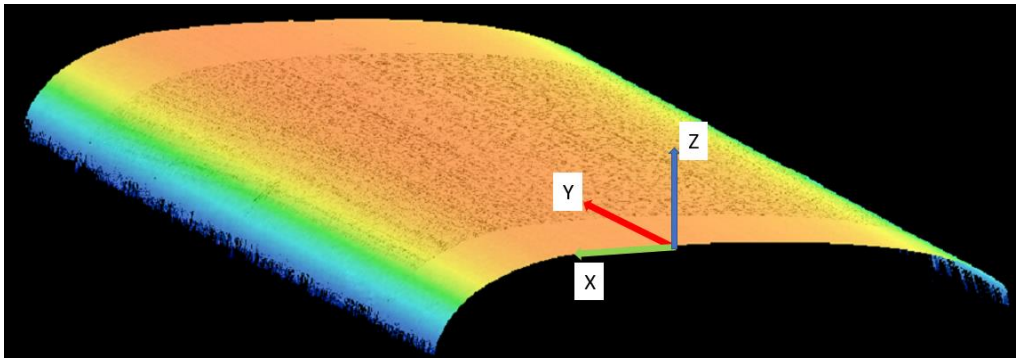

Figure 5.7: 3D coordinates system of the laser profiler.

The coordinates of the longitudinal profile of the peak are required to compute the curvature of the top of rail. Figure 5.7 shows the coordinate system of the laser profiler. Thus, to obtain the longitudinal profile, the next step in the processing is plotting the *Z* coordinate as a function of the *Y* coordinate. The plot is illustrated in Figure 5.8.

The last step is fitting a quadratic polynomial trendline in the longitudinal profile plot of the top of the rail peak (Figure 5.8) and obtaining the second derivative of that equation. The resulting value is the curvature obtained from one scan. To measure the RNT is necessary to repeat this procedure for at least one more dataset (scan and temperature at which the scan was acquired) and finally plot the *curvature (k)* as a function of the *temperature(T)* as described in Knopf et al. [7].

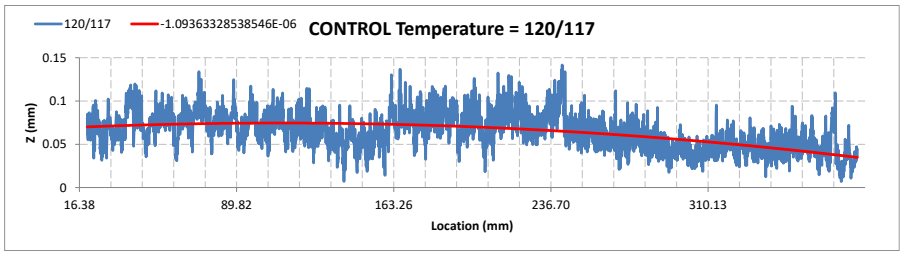

Figure 5.8: Plot of the *Y vs Z* coordinates of peak line of the top of rail.

CHAPTER 6

LABORATORY IMPLEMENTATION & VALIDATION

Testing the system in the laboratory aims to test the adequacy of the system in the proposed method and identify improvement points before testing in the field. Furthermore, the laboratory is a controlled environment regarding lighting and temperature conditions. It also does not have time constraints, so the test can take as long as needed and can be repeated.

6.1 Test Setup

The test consisted of acquiring measurements of rail segment number 3 using the setup illustrated in Figure 6.1. The test started at room temperature (68 degrees Fahrenheit), and the heaters heated the rail to 141 degrees Fahrenheit. The proposed method's hypothesis is based on the constraints of the rail imposed by the track, and the longitudinal continuity of CWR [5, 6, 7]. To produce the longitudinal constraint of CWR in the laboratory, a compressive force of 20 kips was applied to the rail by a hydraulic jack.

Figure 6.1: Rail segments in the laboratory.

Figure 6.2:Hydraulic jack to apply axial compressive force to the rail.

The heaters were placed on the track so that the entire track was heated evenly with the objective of making the longitudinal force in the rail increase linearly with temperature. There were load cells on the edges of the tested rail to measure the axial force in the rail during the test. Figure 6.3 presents the plot of the axial force in the rail as a function of the elapsed test time.

The interpretation of the graph indicates that in the first 15 minutes the axial force did not increase and was near 20 kips, which is the initial force applied on the rail. During the application of the initial compressive force, it is possible to hear the track shifting by the sound of the ballast moving. It means that as force is applied to the system (track), it finds a stable position before it engages to support the applied axial load. In the next 60 minutes, the internal force in the rail varies linearly with the temperature, as desired. Furthermore, between 75 and 95 minutes the system readjusts one more time, dropping the internal forces in the rail. From 95 to 140 minutes, the linear variation is once more observed. In summary, data acquired in the first 15 minutes, and from 75 to 95 minutes, might be unreliable.

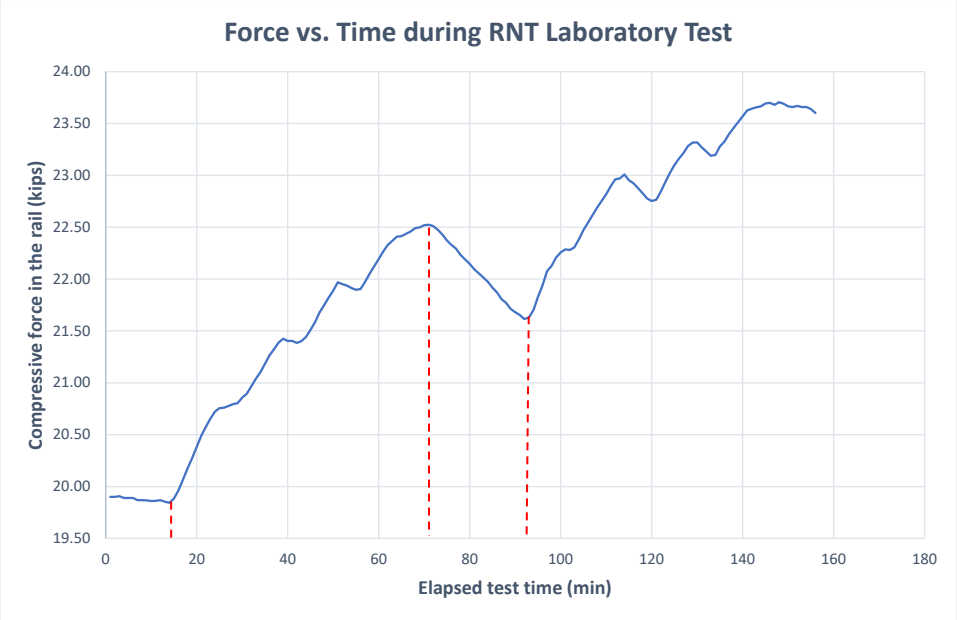

Figure 6.3: Plot of the axial force in the rail as a function of the elapsed test time.

The system setup is the same as discussed in chapter four, and the data acquisition and processing processes applied in the test are the same as the ones described in chapter five.

Figure 6.4: Laboratory Test Setup.

6.2 Testing Procedure & Data Acquisition

The testing procedure involved acquiring data sets for every 10 ^{o}F temperature increase relative to the previous acquisition's temperature. So, for example, the first acquisition was at 68 degrees (baseline), and the next was at 79 degrees.

At every acquisition, three shape measurements of the top of rail were acquired in the same direction, not back and forth. In addition, the temperature was measured before and after acquiring the shape measurements. Figure 6.5 illustrates the shape measurement acquisition process in the laboratory.

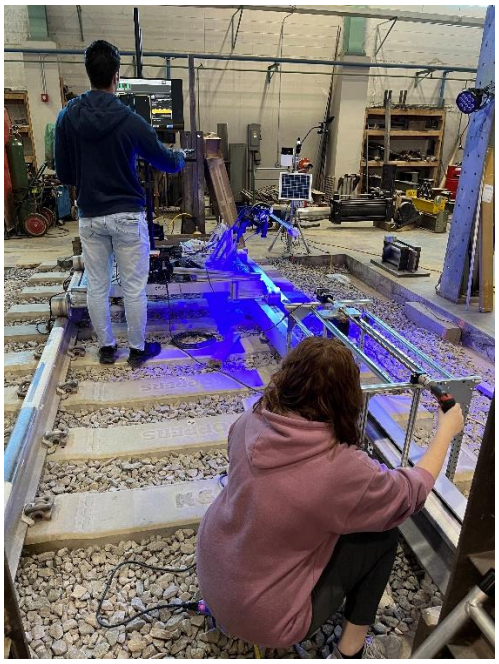

Figure 6.5: Shape measurement acquisition in the laboratory.

Eight data sets were acquired at temperature increment of about 10 ^{o}F and rail segment #3 (Figure 6.1) was scanned 3 times at each temperature for a total of twenty-four shape measurements in the test. The data acquired in each scan is separated into folders in the system controller box. In the folder of each segment, there is a file for each scan. The curvature of each profile is estimated as discussed above and the results are shown in Table 6.1. It is observed that the curvature values in each set are consistent with only a few exceptions. In data sets five, six, seven, and eight, the "---" in the curvature column means no good measurement from that scan, so they were discarded from the correlation. Figure 6.6 shows the profiles acquired in dataset five with similar curvature measurements.

6.3 Results

Table 6.1: Curvature and Temperature measurements obtained in the laboratory test.

Set	Folder	Time	Temperature (F)			Curvature * 10-6 (1/mm)	
			Before	After	Average	Obtained	Average
1	2	1:06:00 PM	68	68	68	-0.91582	-0.84783
	3	1:09 PM				-0.65710	
	4	1:10 PM				-0.97057	
2	5	1:24:00 PM	79	79.9	79.45	-0.81598	-0.99510
	6	1:25 PM				-1.10420	
	7	1:26 PM				-1.06511	
3	8	1:39:00 PM	89.1	88	88.55	-0.95070	-0.77298
	9	1:40 PM				-0.88444	
	10	1:41 PM				-0.48380	
4	11	1:51:00 PM	102	101	101.5	-0.92441	-0.95776
	12	1:52 PM				-0.73706	
	13	1:53 PM				-1.21181	
5	14	2:36:00 PM	110	109	109.5	-1.38974	-1.31230
	15	2:39 PM				-1.23487	
	16	2:41 PM				---	
6	17	2:56:00 PM	120	117	118.5	---	-1.07825
	18	2:57 PM				-1.06287	
	19	2:58 PM				-1.09363	
7	20	3:08:00 PM	132	130	131	-1.68939	-1.63796
	21	3:09 PM				---	
	22	3:10 PM				-1.58653	
8	23	3:23:00 PM	141		141	---	-1.69291
	24	3:24 PM				-1.60375	
	25	3:25 PM				-1.78207	

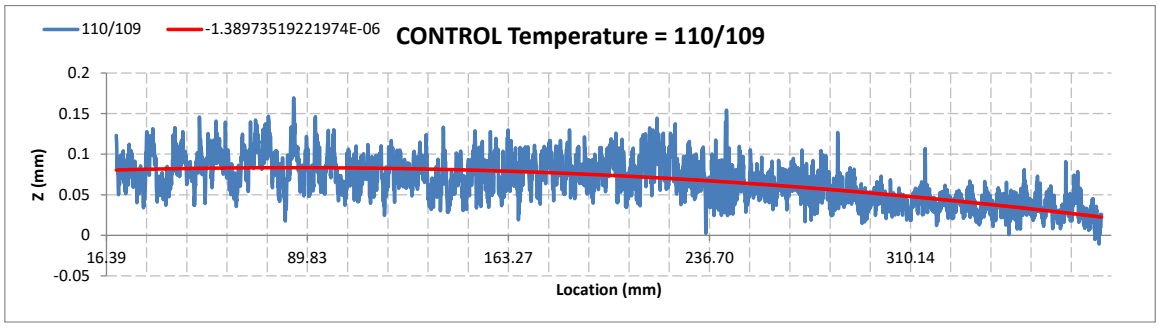

(a)

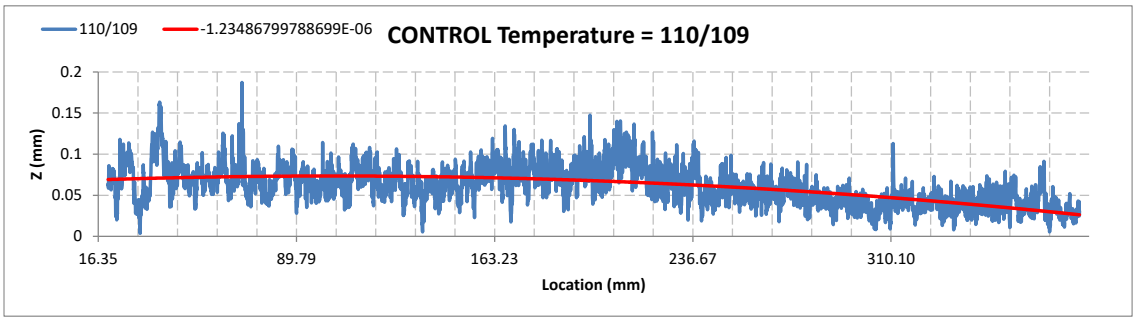

(b)

Figure 6.6: (a) first scan of data set 5 and (b) second scan of data set 5.

Table 6.2 summarizes data used to estimate the RNT. The curvature values are the average of the curvature values obtained in each data set, and the temperature values are the average of the temperature measurements before and after data acquisition.

Table 6.2: Curvature (k) and Temperature (T) for RNT correlation.

Set	Correlation Data	
	Curvature (1/mm)	Temperature (F)
1	-0.84783	68
2	-0.99510	79.45
3	-0.77298	88.55
4	-0.95776	101.5
5	-1.31230	109.5
6	-1.07825	118.5
7	-1.63796	131
8	-1.69291	141

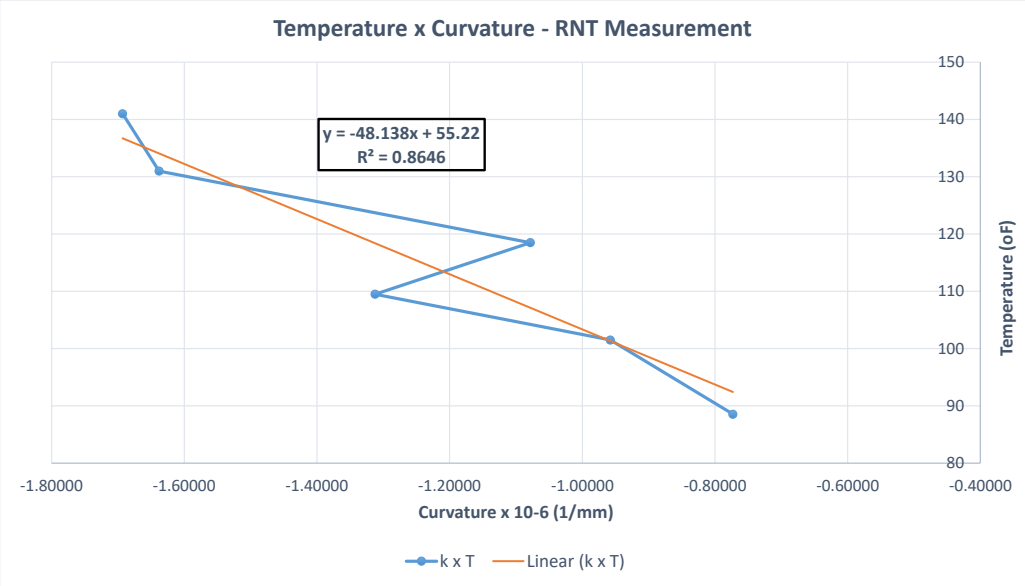

Figure 6.7: Curvature (k) vs. Temperature (T) graph and RNT measurement.

In the correlation presented in Figure 6.7, data from the first two data sets was discarded. As the rail heats and expands it engages the supports at the edges. However, in the first temperatures sets, it is possible to notice the track shifting by the sound of the ballast moving. When the track gets to a stable position, the internal force in the rail starts varying linearly with the temperature, which is expected based on the method's hypothesis [5, 6, 7]. It is also possible to notice the track lost some engagement between sets five and six because the curvatures decreased, disturbing the linearity between curvature and temperature. However, there is an acceptable correlation between curvature and temperature, and the RNT measurement of 55 ^{o}F is acceptable given the estimated RNT of 60 ^{o}F in the laboratory track for this test. Therefore, the laser profiler system can measure

shape coordinates with acceptable noise and repeatability, which leads to good RNT measurements in the laboratory.

The calculation of the RNT in the laboratory track follows the principle of thermal expansion of materials (equation 6.1), and Hooke's law (equation 6.3 & 6.5). The relationship between the internal axial stress in the rail and the temperature (equation 6.4) is obtained substituting equation 6.2 in equation 6.3. Finally, the equation that relates the internal force in the rail to the temperature variation (equation 6.6) is achieved by substituting equation 6.5 into 6.4. Table 6.3 summarizes the parameters to substitute in equation 6.6 to estimate the temperature variation. Once the temperature variation is calculated in equation 6.6, it is trivial to obtain the RNT with equation 6.7.

$$\Delta L = L_0 . \Delta T_0 . \alpha \quad (6.1)$$

$$\varepsilon = \frac{\Delta L}{L_0} = \Delta T_0 . \alpha \quad (6.2)$$

$$\sigma_T = E . \varepsilon_T \quad (6.3)$$

$$\sigma_T = E . \Delta T_0 . \alpha \quad (6.4)$$

$$N_T = -\sigma_T . A \quad \therefore \sigma_T = \frac{-N_T}{A} \quad (6.5)$$

$$N_T = -E . A . \alpha . \Delta T_0 \therefore \Delta T_0 = \frac{-N_T}{E . A . \alpha} \quad (6.6)$$

$$\Delta T_0 = T_{ROOM} - T_{RNT} \therefore T_{RNT} = T_{ROOM} - \Delta T_0 \quad (6.7)$$

Table 6.3: Parameters in the RNT calculation.

Parameters	
E (ksi)	29000
α(1/ °F)	0.0000065
A (in^2)	12.95
N_T (kips)	20

As mentioned in the test setup section of this chapter, the room temperature was sixty-eight degrees Fahrenheit. At that temperature, the internal axial force in the rail was the initial force applied by the hydraulic jack to simulate the longitudinal continuity of CWR. The calculation proceeds with equations 6.8 and 6.9.

$$\Delta T_0 = \frac{-N_T}{E.A.\alpha} = \frac{-(-20)}{(29000).(12.95).(0.0000065)} = 8.19 \cong 8°\text{F} \quad (6.8)$$

$$T_{RNT} = T_{ROOM} - \Delta T_0 = 68 - 8 = 60°\text{F} \quad (6.9)$$

CHAPTER 7

FIELD IMPLEMENTATION

The field implementation of the system discussed in Chapters 4 and 5 aims to assess the effects of field conditions on the measurements, and to identify weaknesses and areas of improvement both in the hardware setup, testing procedures, and data processing.

7.1 Description of the Site

The site selected is a CSX track at Alpine Road in Columbia, South Carolina. Figure 7.1 shows an aerial view of the site. The site consists of a RE115 CWR track on timber ties with a desired RNT of 105 ◦F, illustrated in Figure 7.2.

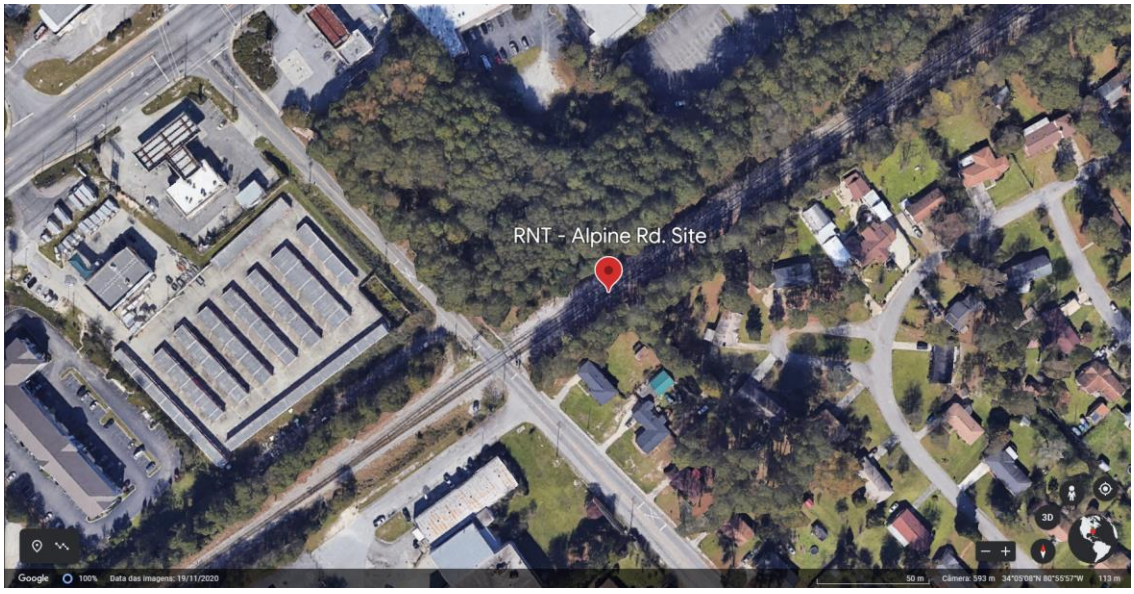

Figure 7.1: Satellite image of the test site

Figure 7.2: CSX CWR track on timber ties.

7.2 Rail Preparation & Setup

The test consisted of scanning five rail segments along the track as many times as possible in the time frame CSX granted access to the track. The temperature change between sets must be between seven and twelve degrees Fahrenheit, and the overall temperature must vary at least 15 degrees.

Once the test location in the site was selected, three heaters were placed with no space between them, and five rail segments were selected according to the scheme in Figure 7.3. After that, the rail segments were wiped, and the markings were drawn on the top of the rail segments.

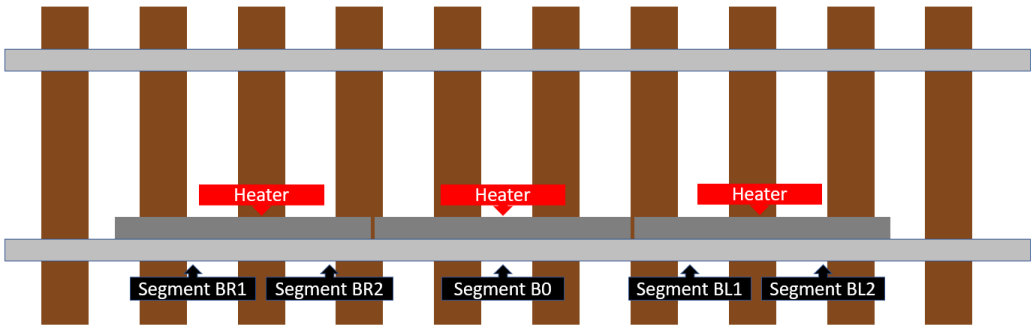

Figure 7.3: RNT field test scheme

The markings are the edge of the ties, the tie space center, eight inches from the center in both directions and the center of the top of the rail, as illustrated in Figure 7.4. The purpose of the markings is to guide the laser operator in setting the laser to the proper initial position so that data is acquired relating to the center of the top of the rail and the entire sixteen inches of scanning capacity is well used. Also, they serve as a guide when using the simulation software during the offline data processing if necessary.

Figure 7.4: Markings on the top of rail segment.

The setup consists of the one described in chapter four. In addition, shades were applied on top of rail to avoid reflections in the laser during data acquisition. Figure 7.5 shows the setup assembled in the field. Also, Figure 7.6 presents the frame on a rail segment ready to take measurements.

Figure 7.5: RNT field test setup of the laser profiler.

Figure 7.6: Laser Profiler ready to take measurements in the field.

7.3 Testing Procedure & Data Acquisition

The testing procedure to acquire a data set for a rail segment consisted of placing the frame on a rail segment and adjusting it so that the frame is steady and leveled. The next step was measuring the temperature and acquiring shape measurements with the laser profiler.

Figure 7.7: Placing and adjusting the frame on a segment of rail.

Figure 7.8: Measuring the temperature.

In between measurements, measuring the temperature in the rail segments was necessary to monitor the temperature variation. When the temperature rose seven to twelve degrees in a segment, it was time to acquire a new dataset.

In the test, the scanning direction was from segment BR1 to BL2. Usually, when a dataset in segment BL2 was acquired, the temperature in segment BR1 rose by the desired amount, so it was time to take another set of measurements.

Six data sets were acquired in each rail segment, for a total of thirty datasets in the test. The data acquired in each segment is separated into folders in the system controller box. In the folder of each segment, there is a file for each measurement.

During the test, after acquisition of dataset four a train passed on the track, affecting the conditions of the internal forces in the CWR track. Therefore, the sets acquired after the train are number in a different way than the previous sets, as seen in Table 7.1.

7.4 Results

Table 7.1: Curvature (k) and Temperature (T) measurements obtained in the field test for segment B0.

Segment B0				
set	Curvature x10-6 (1/mm)		Temperature (oF)	
	forward	backward	Web	TOR
1	0.881968	0.9500403	61.7	62.5
2	0.755878	-0.0521222	76.5	80
3	0.306745	-0.258104	85	90
4	-0.382545	-0.0500168	98	101
t1	-1.714651	-1.3415355	94.3	94.8
t2	0.0013883	3.747464	112	118

Analyzing Table 7.1, the laser profiler system could not measure similar enough curvatures in the forward and backward scans (besides sets 1 and t1), as unexpected because the system scanned the same rail segment. The “t” before “t1” and “t2” means sets after a train passed on the track.

Figure 7.9 presents the profiles acquired in data set 1 of segment B0. It is possible to notice the outliers in the data that are affecting the curvature measurement. Also, the forward and backwards scans are mirrored and not centered in relation to the same point. Therefore, the curvature values computed are for slightly different rail segments.

Figure 7.10 shows the graphs of curvature versus temperature. There are different correlations for the forwards and backwards scans because of the significant difference in the curvature values. Also, data acquired before and after the train passed on the track cannot be correlated together because the train affects the internal forces in the rail. The RNT measurement for segment B0 is not acceptable, as expected based on the unreliable data used in the inputs.

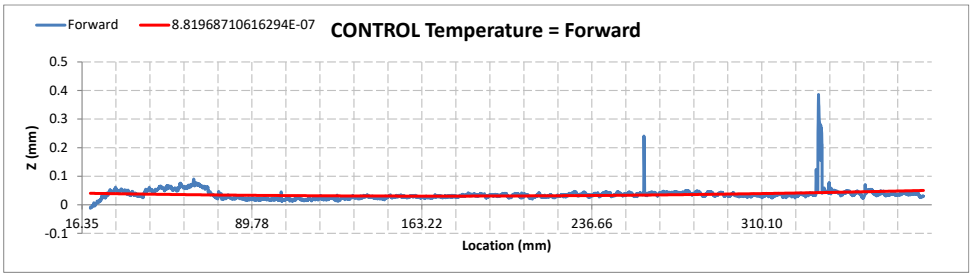

(a)

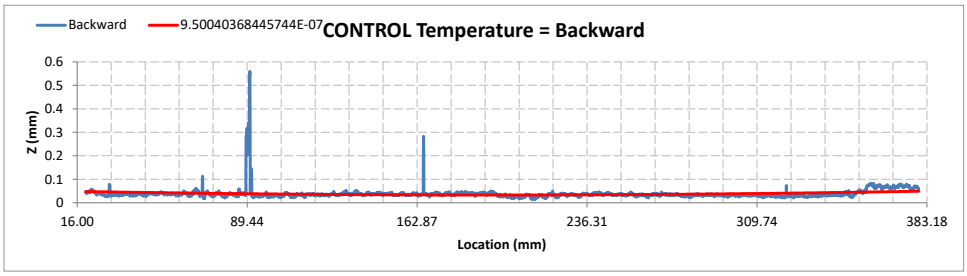

(b)

Figure 7.9: Profiles acquired in data set 1 of segment B0 in the (a) forward and (b) backwards direction.

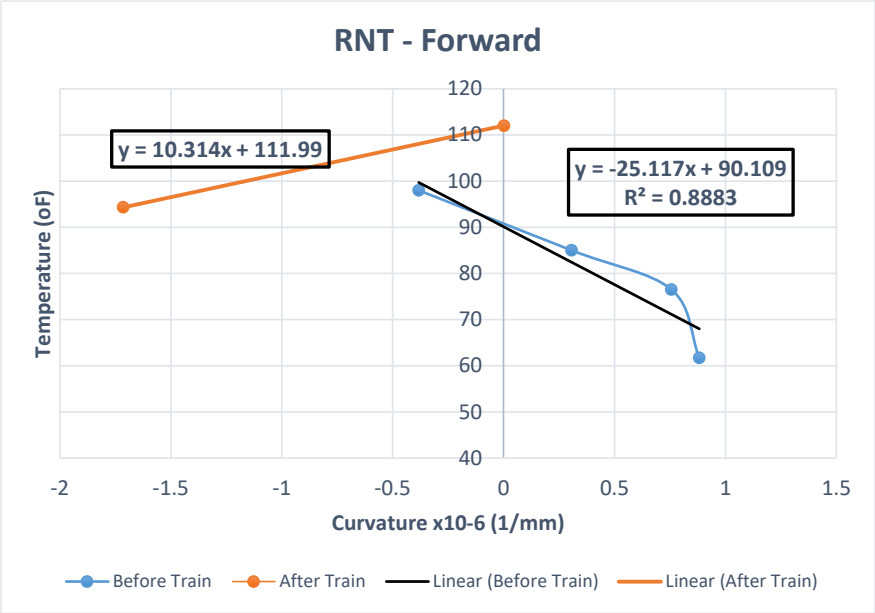

(a)

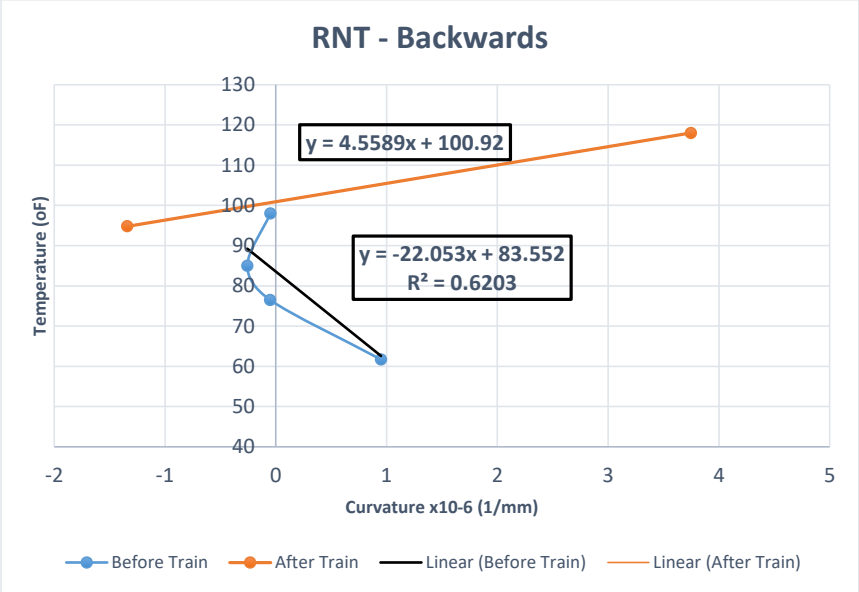

(b)

Figure 7.10: RNT measurement using curvature values from (a) Forward and (b) Backwards scans.

The spikes observed in the scans -probably originated from brighter lighting conditions of the field- are outliers in the data, affecting the quadratic curve fitting, which also affects the curvature measurements. Therefore, a filter is applied to the data before computing the curvature.

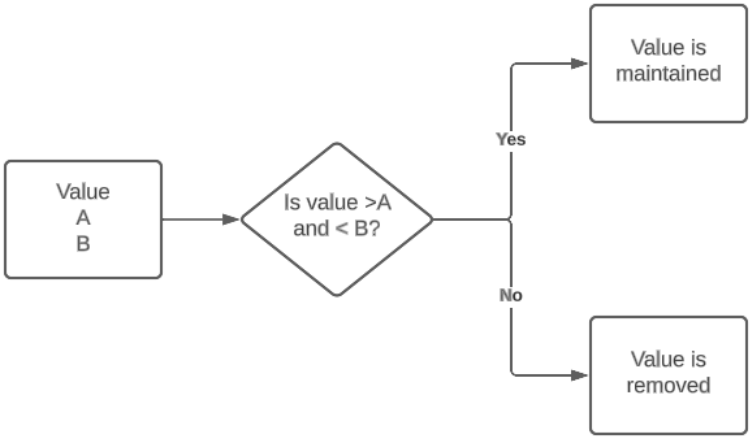

Figure 7.11:Flowchart of the filter to eliminate outliers.

$$Z_{AVG} = \sum_{i}^{n} \frac{z_i}{n} \; \forall \; 0 \leq y \leq L \tag{7.1}$$

$$Z = \begin{cases} Z_i, |Z_{AVG} - 1\ std| \leq |Z_i| \leq |Z_{AVG} + 1\ std| \\ Removed, \left|Z_{AVG} \quad + 1\ std\right| \leq |Z_i| \leq |Z_{AVG} - 1\ std| \end{cases} \tag{7.2}$$

Figure 7.11 presents the flowchart. In the chart, A represents the average Z minus one standard deviation, B stands for the average Z plus one standard deviation. Equations 7.1 and 7.2 described the filter. Figure 7.12 illustrates the difference between the original and filtered scans.

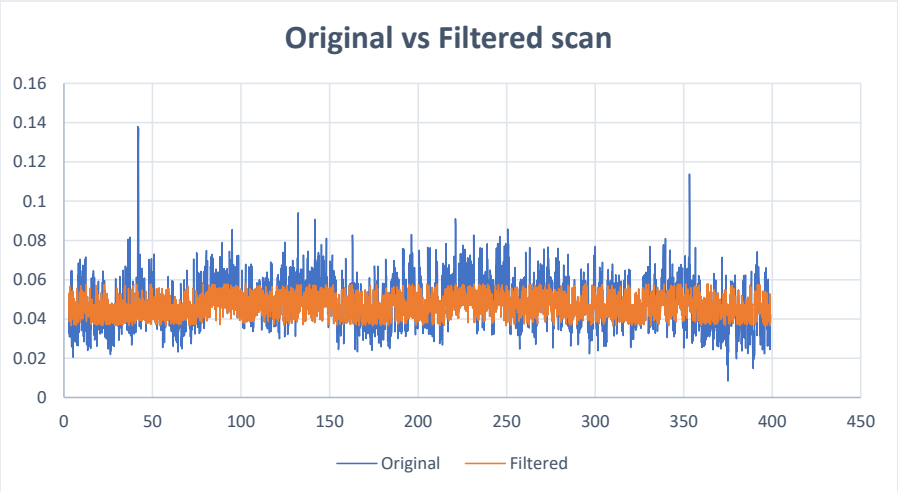

Figure 7.12: Original vs filtered scan.

In addition to removing the outliers, the axial coordinate (y in the laser coordinate system) was adjusted so that the forward and backwards scans are centered. To make sure the curvature values were computed from the same segment of rail, a range of -90mm to 90mm were used to fit the quadratic curve in relation to the center of the acquired shape. To adjust the y coordinate of the center, all the y coordinate values were subtracted from the y coordinate of the center. The simulation software was used to acquire the values of the y coordinate of the center of the shape measurement.

Table 7.2: Y coordinate of the center of the acquired scans of the segment B0 data sets.

set	Axial coordinate of the center of the profile (mm)	
	forward	backward
1	227	195
2	222	205
3	224	188
4	224	196
t1	215	204
t2	223	219

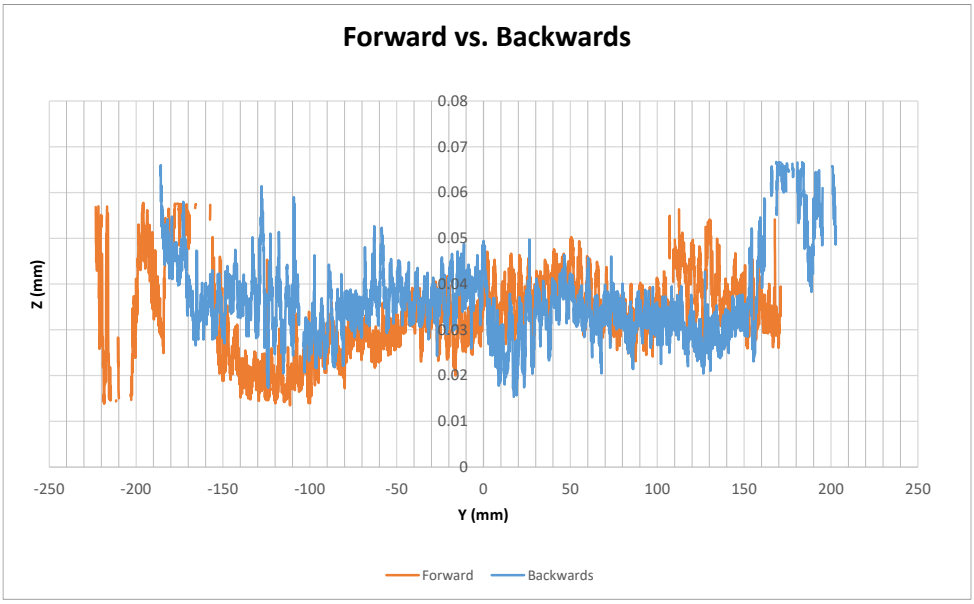

Figure 7.13: Graph of the forward and backwards scans of the first data set of segment B0.

Figure 7.13 presents the plots of the scans acquired in the first data set of segment B0. It is possible to notice the profiles are mirrored and that the scans are not exactly similar. This graph indicates that during the acquisition of the shape measurement in the forward direction, the laser head stopped 3.2 cm after the correct stop position. Therefore, the backwards scan acquisition 3.2 cm before the initial position of the forward scan. Also, although the outliers were removed, there is still considerable noise in the measurements.

Figure 7.14 illustrates the scans used to compute the curvature in the first dataset of segment B0. The same approach was applied to the remaining data sets to measure RNT. Analyzing the graph, one can notice the profiles are mirrored, but different, against expectations. This is also evidenced by the quadratic fitting of both scans because they are also clearly different. As expected, and presented in, the curvatures are different and the RNT correlation is unsatisfactory.

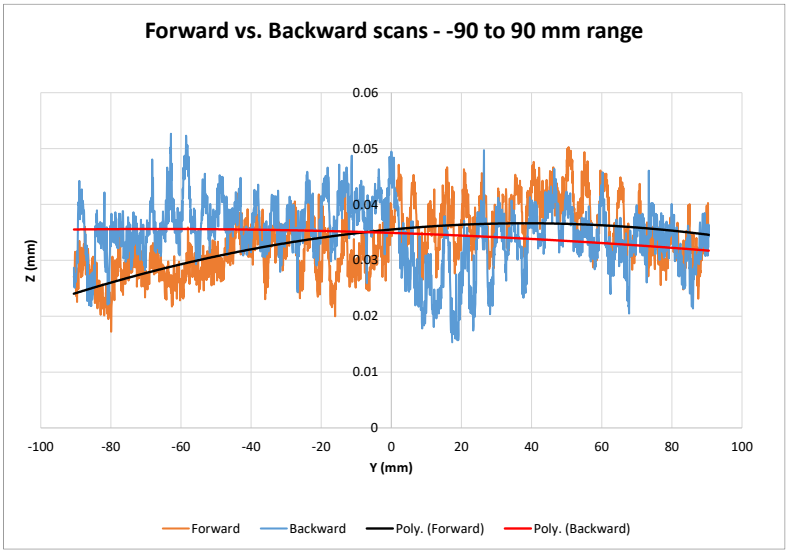

Figure 7.14: Forward vs. Backwards scan in a range from -90mm to 90mm.

Table 7.3: Curvature(k) and Temperature(T) data obtained after filtering and adjusting the data.

Set		Curvature *10-6 (1/mm)		
	Temperature (*F)	Forward	Backward	Average
1	61.7	-0.156311	-0.757252	-0.45678
2	76.5	-0.218795	-0.891344	-0.55507
3	85	-0.992782	-0.558837	-0.77581
4	98	-1.04027	-0.581492	-0.81088
t1	94.3	-0.616757	-0.319978	-0.46837
t2	112	0.00140675	-0.27831	-0.13845

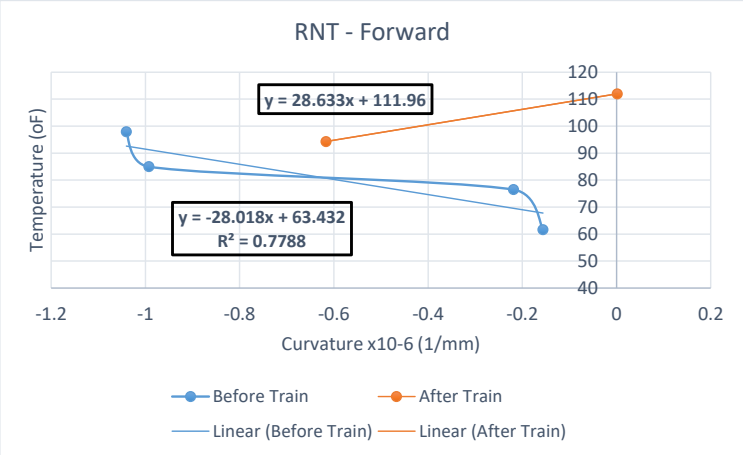

(a)

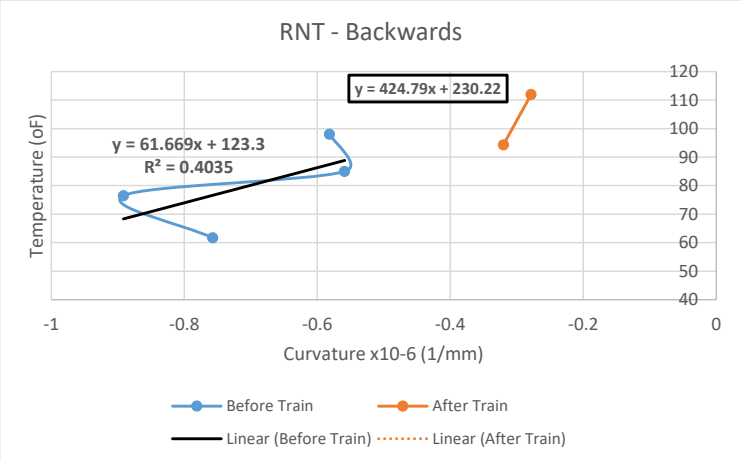

(b)

Figure 7.15: RNT measurement using curvature values from (a) Forward and (b) Backwards scans.

As expected, the RNT measurement is not reliable because the shape measurements are not reliable either. The curvature does not vary linearly with the temperature, as states the method concept [5, 6, 7]. In the forward scans correlation after the train passes, the RNT estimated is close to the expected value, but more points are needed to judge the linearity between curvature and temperature.

CHAPTER 8

DISCUSSION

Noise is unavoidable in data acquisition systems and comes from many sources. In the case of this project, some noise sources are the system itself, the frame's vibration that comes from the current laser head driving system, lighting conditions, and rail wear.

The shape measurements acquired in different data sets for segment B0 are presented in Figure 8.1. The noise in the measurements may have a different pattern across different scans. It excludes rail corrugation as a significant noise source in the measurements because otherwise, the patterns would be the same across different scans and data sets.

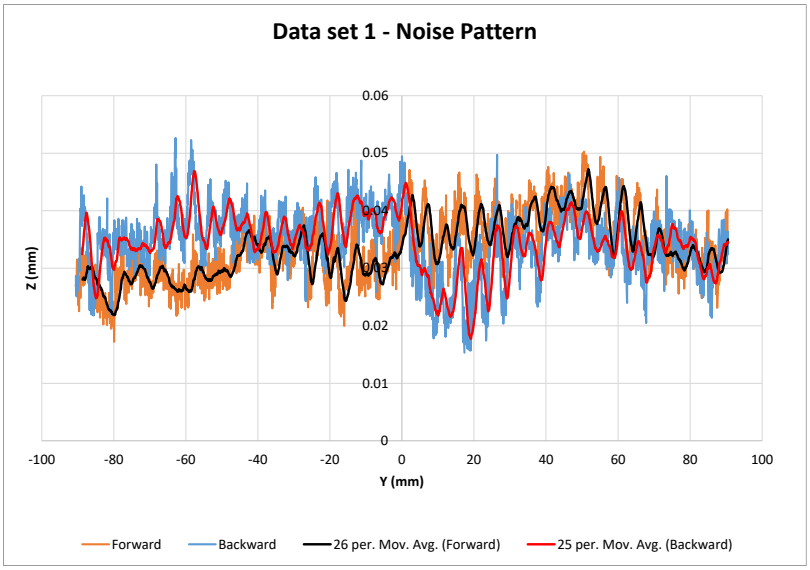

(a)

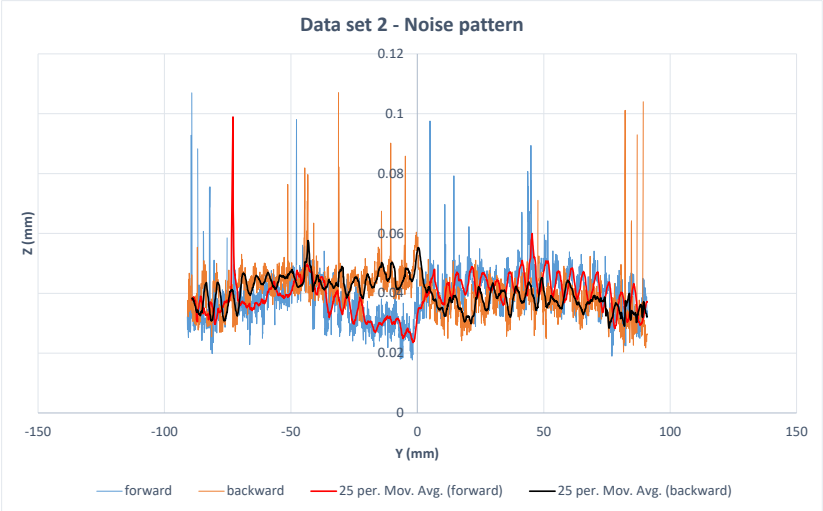

(b)

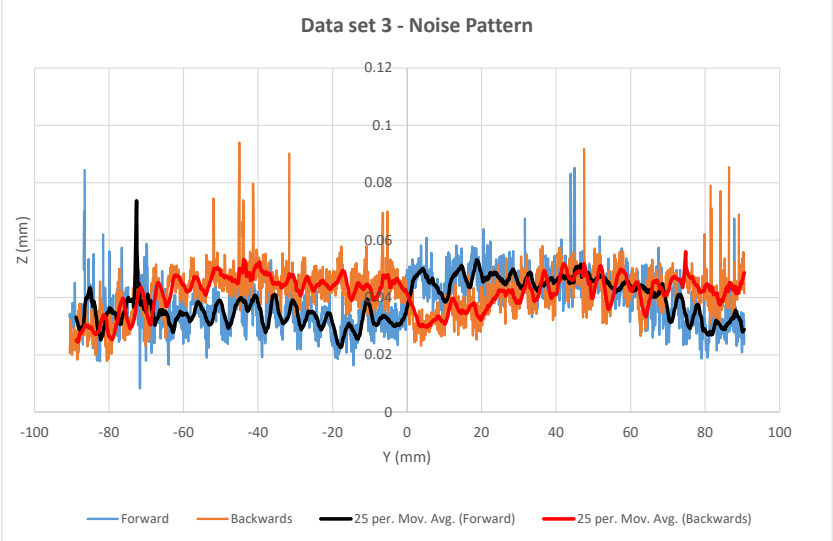

(c)

Figure 8.1: Noise pattern in (a) data set 1, (b) data set 2, and (c) data set 3 acquired in segment B0.

The moving average trendline eliminates the random noise but reveals a sine wave varying its pattern in every shape measurement. Another aspect of the sine wave is that its amplitude varies, but the frequency seems constant throughout the profile.

Fast Fourier transformation (FFT) was applied to three scans acquired in the field, laboratory, and flatness verification tests to assess the frequencies in the shape measurements. The shape measurements of the laboratory and field test are from the top of the rail, and the measurement of the flatness verification is from the granite slab.

The amplitude spectrums in Figure 8.2, Figure 8.3, and Figure 8.4 indicate two frequencies with high predominance in the shape measurements in the field and in the flatness measurements in the laboratory. The greater one is the frequency of the shape itself, and the second one is the noise that highly affects the field measurements. The secondary frequency is not relevant in the top of rail shape measurements acquired in the laboratory, as expected in valid measurements. However, the fact that this frequency is predominant both in the field and the flatness measurements in the laboratory indicates that the source of the noise is more likely to be the current setup to acquire data with the laser instead of sources present in the field environment, such as lighting conditions and reflections of the sunlight on the top of rail surface.

It was stated in chapter four that the frame is susceptible to vibrations. Driving the laser with the power drill on a ball screw introduces vibration in the frame, especially because the ball screw was turned to reduce the diameter to fit the coupler to the power drill. There is an eccentricity that resulted from this process that makes the entire frame vibrate both in the longitudinal and vertical directions at every revolution.

Additionally, in the field, five different segments were scanned, and moving the frame constantly on the track may have affected the stability of the frame. The secondary frequency is at 0.2 Hz. It means the period is 5 millimeters, as calculated in equation 8.1. The scan acquired in the field test used to measure RNT is 180 millimeters long. Hence, if the period is 5 millimeters, 36 peaks are expected in the moving average sine pattern, according to equation 8.2. It is possible to count 35 peaks in the moving average line of the forward profile, confirming the 5 millimeters period. The lead of the ball screw (linear travel of the laser head per rotation of the ball screw) is 5 millimeters. Therefore, it is confirmed that the 0.2 Hz frequency noise affecting the measurements comes from the vibration of the frame.

$$T = \frac{1}{f} = \frac{1}{0.2} = 5\ mm \quad (8.1)$$

$$Peaks = \frac{Length}{T} = \frac{180}{5} = 36 \quad (8.2)$$

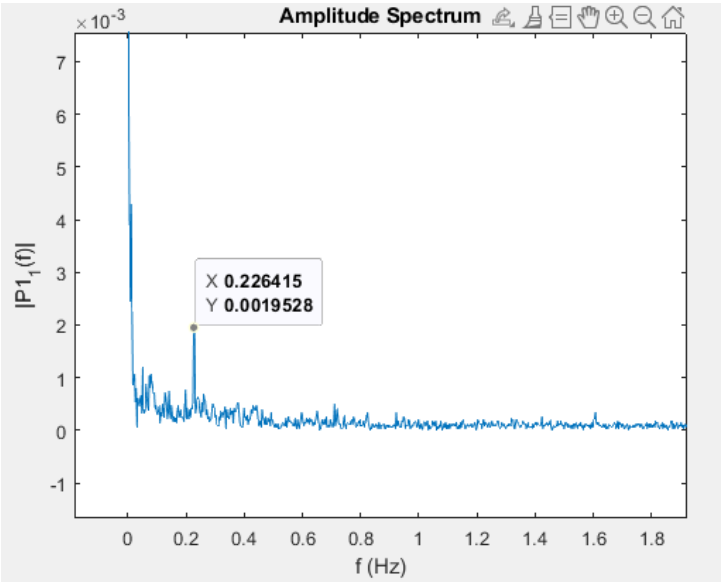

Figure 8.2: Amplitude spectrum of frequencies in the field test shape.

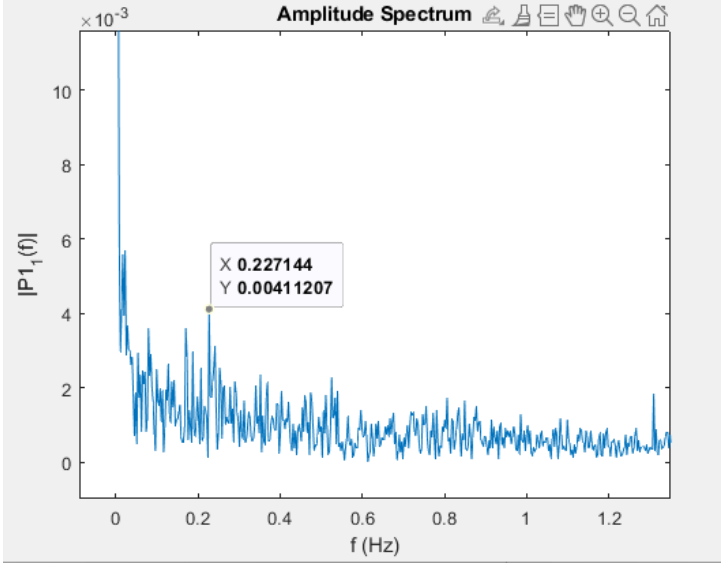

Figure 8.3:Amplitude spectrum of frequencies in the laboratory test shape.

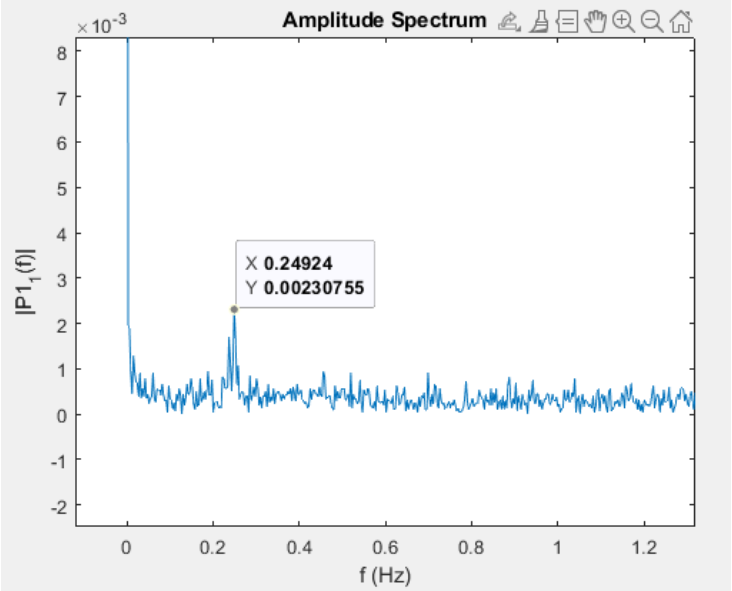

Figure 8.4 Amplitude spectrum of frequencies in the granite slab shape measurement in the longitudinal direction.

Although the frame vibrations are inherent to the setup, in the laboratory test, an assistant held the frame steady, which was impossible in the field test. On top of that, the laboratory is a controlled environment, as opposed to the field, so the noises in the laboratory tend to be easier to deal with. Furthermore, in the flatness measurements, although the 0.2 Hz frequency is present, the quadratic fitting averages out the noise from the vibrations. Therefore, the curvature in the flatness measurements is not affected by the noise. However, as illustrated in Figure 8.5, the twenty points moving average eliminates the random noise and reveals the peaks caused by the 0.2 Hz frequency noise. That explains why the system worked in the laboratory to measure the flatness of the granite slab and RNT with reliable shape measurements.

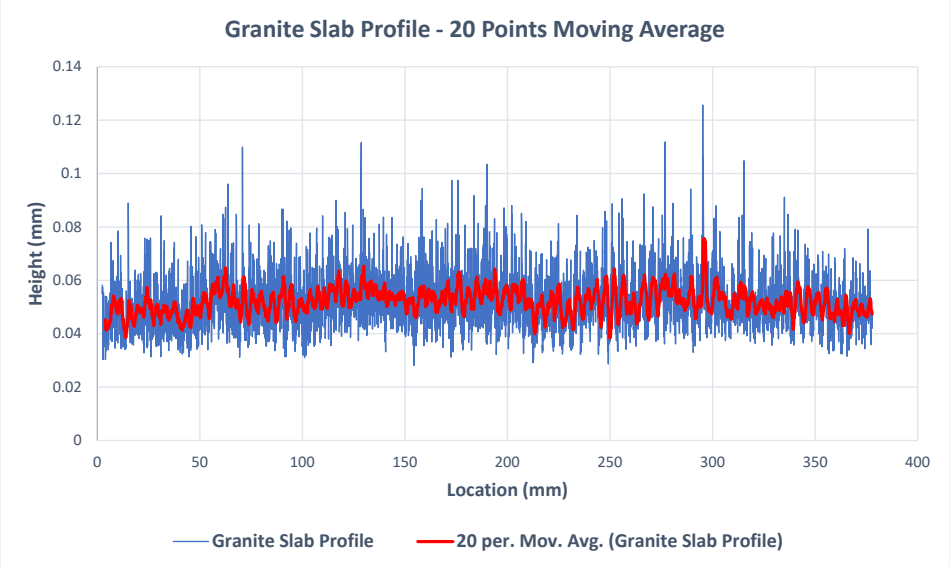

Figure 8.5: Granite Slab Profile in the Longitudinal Direction with 20 Points Moving Average.

CHAPTER 9

CONCLUSION

The objective of this thesis is to develop the implementation process of a 3D laser profiler into the RNT measurement methodology proposed in [5]. It describes all the steps from the conception, design, and assembly of the work frame to the field implementation and final configurations of the equipment. Also, it comments on the advantages the equipment brought to the methodology, identifies areas of improvement and lists recommendations for future work.

The laser profiler works for the proposed concept to measure RNT as it can acquire reliable shape measurements. However, it still needs to get reliable data out in the field. The system is envisioned to be coupled with other systems to form an efficient and portable product to measure RNT and the stress state in CWR track rails successfully implemented in the industry.

It was found in the discussion chapter that there is noise in the measurements coming from the vibration of the frame. Further investigation in the data acquired in the field test is applying inverse Fourier transformation to remove the undesired frequencies from the profile, therefore eliminating the noise. It should return the actual measured shape of the top of rail to compute the curvatures and measure RNT.

Additionally, future implementation in the project is designing new instrumentation for the system to reduce the noise in the field measurements. In addition, it is necessary to have better control of the starting and stopping positions of the laser head to ensure the system is scanning the same part of the rail segment.

In the current setup, the frame is static as the laser moves on top of it. If the same concept is used, the motion system should be smooth and the setup rigid because the laser head cannot oscillate while taking measurements.

An alternative concept is designing instrumentation in which the laser head is static, and the setup moves to drive it. For example, a structure to attach the laser head to a rail cart while all the system components are on it would allow quickly acquiring measurements in multiple rail segments. On top of that, it would eliminate noise from driving the laser head.

The 3D laser profiler works in the proposed method to measure RNT but still needs further validation in the field. A suggestion to achieve it is improving the instrumentation to reduce the noise in the measurements to acquire good data in the field.

REFERENCES

[1] Federal Railroad Administration, "Track Buckling Prevention: Theory, Safety, Concepts, and Applications," 2013.

[2] A. Kish, "Best Practices Guidelines for CWR Neutral Temperatue Management," in *AREMA*, 2013.

[3] U.S. Department of Transportation, "DOT Open Data Catalog," 2023. [Online]. Available: https://data.transportation.gov/Railroads/Rail-Equipment-Accident-Incident-Data/85tf-25kj/data. [Accessed 16 May 2023].

[4] J. A. e. a. Zakeri, "New Definition of Neutral Temperature in Continuous Welded Railway Track Curves," *Periodica Polytechnica Civil Engineering,* vol. 62(1), p. 5, 2018.

[5] D. Rizos, E. Chao, B. Stinson, C. Penna, M. Sutton and R. Wilson, "Reference-Free Procedure for RNT and Longitudinal Stress Measurements: Field Implementation and Validation.," in *AREMA*, 2022.

[6] K. Knopf, D. Rizos, Y. Qian and M. Sutton, "A Non-Contacting System for Rail Neutral Temperature and Stress Measurements," *Structural Health Monitoring,* p. 17, 2020.

[7] e. a. Knopf, "A Stereovision System for Rail Neutral Temperature Measurements and Effects of the Heating Method.," in *AREMA*, 2020.

[8] E. Chao, "Development of a First-Generation Prototype Laboratory System for Rail Neutral Temperature Measurements," 2019.

[9] A. Enshaeian and P. Rizzo, "Stability of Continuous Welded Rails: A State-of-the-art Review of Structural Modeling and Nondestructive Evaluation," *Journal of Rail and Rapid Transit,* pp. 1-21, 2021.

[10] M. Belding, A. Enshaeian and P. Rizzo, "Vibration-Based Approach to Measure Rail Stress: Modeling and First Field Test," *Sensors,* no. 22, 2022.

[11] W. e. al., "Rail Neutral Temperature Estimation using Impulse Vibration and Machine Learning," in *SPIE*, 2021.

[12] J. Ye, E. Stewart and C. Roberts, "Use of a 3D Model to Improve the Performance of Laser-Based Railway Track," in *Institution of Mechanical Engineers*, 2019.

[13] J. Ye, E. Stewart, D. Zhang, Q. Chen, K. Thangarai and C. Roberts, "An Integration of Multiple Sensors for Noncontact Rail Profile Measurement and Inspection.," *IEEE Transactions on Instrumentation and Measurement,* vol. 70, p. 12, 2021.

[14] Y. Yang, L. Liu, B. Yi and L. CHen, "An Accurate and Fast Method to Inspect Rail Wear Based on Revised Global Registration," *IEEE Access,* vol. 6, p. 12, 2018.

[15] H. Liu, Y. Li, Z. Ma and C. Wang, "Recognition and Calibration of Rail Profile Under Affine-Distortion-Based Point Set Mapping," *IEEE Transactions on Instrumentation and Measurement ,* vol. 66, p. 10, 2017.

[16] F. Attivissimo, A. Danese, N. Giaquinto and P. Sforza, "A Railway Measurement System to Evaluate the Wheel-Rail Interaction Quality.," *IEEE Transactions on Instrumentation and Measurement,* vol. 56, p. 7, 2007.

[17] MERMEC, "Infrastructure Monitoring Systems - Railway Infrastructure Manager," [Online]. Available: https://www.mermecgroup.com/press-room/943/resource-library.php/&res=944. [Accessed 19 01 2023].

[18] ENSCO, "Track Inspection Products & Services," [Online]. Available: https://www.ensco.com/rail/rail-profile-measurement-system-rpms. [Accessed 22 01 2023].

[19] M. e. a. Micic, "Inspection of RCF Defects - Review of NDT Methods," *Mechanical Systems and Signal Processing,* vol. 182, p. 24, 2023.

[20] K. Ng, I. Ghafoor and P. Tse, "A Novel Laser-Based Duffing Oscillator System to Identify Weak Ultrasonic Guided Wave Signals Related to Rail Defects," *Optics and Lasers in Engineering,* vol. 157, p. 10, 2022.

[21] S. e. a. Coccia, "USCD/FRA Non-Contact Ultrasonic Guided-Wave System for Rail Inspection: An Update," *Sensors and Smart Structures Technologies for Civil, Mechanical, and Aerospace Systems,* p. 9, 2011.

[22] P. Rizzo, "Sensing Solutions for Assessing and Monitoring Railroad Tracks," Elsevier Ltd, 2014, p. 28.

[23] W. L. D. L. Y. e. a. Chen, "Development and Application of a Multi-sensor Integration Detection and Analysis Device for Metro Gauge and Track Geometry State," *AIP Advances,* p. 14, 2021.

[24] A. e. a. Sanchez-Rodriguez, "Automated Detection and Decomposition of Railway Tunnels from Mobile Laser Scanning Datasets," *Automation in Construction,* vol. 96, p. 9, 2018.

[25] S. e. a. Wang, "Automatic Laser Profile Recognition and Fast Tracking for Structured Light Measurement Using Deep Learning and Template Matching," *Measurement,* vol. 169, 2021.

[26] Q. e. a. Mao, "A Rigorous Fastener Inspection Approach for High-Speed Railway from Structured Light Sensors," *ISPRS Journal of Photogrammetry and Remote Sensing ,* vol. 143, pp. 249-267, 2018.

[27] P. Zhou, K. Xu and D. Wang, "Rail Profile Measurement Based on Line-Structured Light Vision," *IEEE Access,* vol. 6, 2018.

[28] Z. e. a. Liu, "Simple and Fast Rail Wear Measurement Method Based on Structured Light," *Optics and Lasers in Engineering,* vol. 49, pp. 1343-1351, 2011.

[29] Keyence, "Laser Profiler LJ-X8000 Series User's Manual (3D mode)," Keyence.

[30] Keyence, "2D/3D Laser Profiler LJ-X8000 Series High-Resolution Inline Measurement 3200 points/line," Keyence.

[31] H. Yun, K. Lee, Y. Park and D. Jung, "Rail Neutral Temperature Monitoring Using Non-Contact Piezospectroscopy: A Field Study at High-Speed Rail Track," *Construction and Building Materials,* vol. 204, pp. 357-370, 2019.

APPENDIX A: CSV FILE EDITOR CODE

```
# -*- coding: utf-8 -*-
"""
Spyder Editor

This is a temporary script file.
"""

#import csv library
import csv

#Reading the input csv file
f_read = open ('C:/Users/cpenna/OneDrive - University of South Carolina/Civil
Engineering/Master`s Degree/Research Project/Laser
Scanner/WORKSPACE/LAB/03142023/Set 6/230314_145522.csv');
read = csv.reader(f_read);

#Counter to iterate in the data list
encoder = 1

#Header of the new data structre
header = ['X','Y','Z'];

#Create a list of points in which each element is a sublist [X,Y,Z[]
points = list()
for element in read:
    while encoder < len(element):
        pos = list([element[encoder],element[encoder+1],element[encoder+2]])
        points.append(pos)
        encoder = encoder+3

#Rewriting the data in a new structure
f_write = open ('C:/Users/cpenna/OneDrive - University of South Carolina/Civil
Engineering/Master`s Degree/Research Project/Laser
Scanner/WORKSPACE/LAB/03142023/Set
6/230314_145522.csv','w',newline='');
write = csv.writer(f_write);

#Write the header of the new data structure
```

```
write.writerow(header)

#Write the points[X,Y,Z] in a new line
for point in points:
    write.writerow(point)

#Close the csv files
f_read.close()
f_write.close()
```